

The dynamics of CO₂-driven granular flows in gullies on Mars

Lonneke Roelofs ¹, Susan J. Conway ², Bas van Dam ¹, Arjan van Eijk ¹, Jonathan P. Merrison ³, Jens Jacob Iversen ³, Matthew Sylvest ⁴, Manish R. Patel ⁴, Henk Markies ¹, Marcel van Maarseveen ¹, Jim McElwaine ⁵, Maarten G. Kleinhans ¹, Tjalling de Haas¹

¹Department of Physical Geography, Faculty of Geosciences, Utrecht University, Princetonlaan 8a, 3584 CB Utrecht,Netherlands

²Nantes Université, Univ Angers, Le Mans Université, CNRS, Laboratoire de Planétologie et Géosciences,

LPG UMR 6112, 44000 Nantes, France

³Mars Simulation Laboratory, Aarhus University, Ny Munkegade, Bygning 520, 8000 Århus C, Denmark

⁴School of Physical Sciences, The Open University, Milton Keynes, United Kingdom

⁵Department of Earth Sciences, Durham University, Durham, United Kingdom

Key Points:

- The sublimation of small amounts of CO₂ ice can fluidize granular material on low slopes under Martian atmospheric pressure.
- The flow dynamics of CO₂-driven flows are similar to that of terrestrial fluidized two-phase flows, e.g. debris flows and dense pyroclastic flows.
- Experimental CO₂-driven granular flows create deposit morphologies similar to those observed in Martian gullies.

Corresponding author: Lonneke Roelofs, 1.roelofs@uu.nl

21 **Abstract**

22 Martian gullies are landforms consisting of an erosional alcove, a channel, and a depo-
 23 sitional apron. A significant proportion of Martian gullies at the mid-latitudes is active
 24 today. The seasonal sublimation of CO₂ ice has been suggested as a driver behind present-
 25 day gully activity. However, due to a lack of in-situ observations, the actual processes
 26 causing the observed changes remain unresolved. Here, we present results from flume ex-
 27 periments in environmental chambers in which we created CO₂-driven granular flows un-
 28 der Martian atmospheric conditions. Our experiments show that under Martian atmo-
 29 spheric pressure, large amounts of granular material can be fluidized by the sublimation
 30 of small quantities of CO₂ ice in the granular mixture (only 0.5% of the volume fraction
 31 of the flow) under slope angles as low as 10°. Dimensionless scaling of the CO₂-driven
 32 granular flows shows that they are dynamically similar to terrestrial two-phase granu-
 33 lar flows, i.e. debris flows and pyroclastic flows. The similarity in flow dynamics explains
 34 the similarity in deposit morphology with levees and lobes, supporting the hypothesis
 35 that CO₂-driven granular flows on Mars are not merely modifying older landforms, but
 36 they are actively forming them. This has far-reaching implications for the processes thought
 37 to have formed these gullies over time. For other planetary bodies in our solar system,
 38 our experimental results suggest that the existence of gully-like landforms is not neces-
 39 sarily evidence for flowing liquids but that they could also be formed or modified by sublimation-
 40 driven flow processes.

41 **Plain Language Summary**

42 Martian gullies are landforms that look like landforms carved by aqueous debris
 43 flows on Earth. At the top, the gullies have an erosional alcove where material is eroded
 44 and at the bottom of the gully, a fan exists where the eroded material is deposited. For
 45 a long time, it was believed that these gullies were formed by liquid water, just like on
 46 Earth. However, the Martian gullies are active today, which cannot be reconciled with
 47 the low atmospheric pressure and resulting lack of liquid water on the surface of Mars.
 48 Data from satellites has shown that the activity in Martian gullies is correlated to a sea-
 49 sonal cycle of CO₂ ice deposition and sublimation. However, these observations are in-
 50 direct, and therefore, we do not know whether and how CO₂ sublimation produces the
 51 observed changes in gullies. Here we show the results of flume experiments in environ-
 52 mental chambers in which we created CO₂-driven flows under Martian atmospheric con-
 53 ditions. The experiments show that granular material can be fluidized by sublimation
 54 of CO₂ ice. Furthermore, the experimental flow dynamics and morphology of the deposits
 55 are similar to debris flows and pyroclastic flows on Earth. This explains the similarity
 56 between the Martian gullies and the water-shaped gullies on Earth without the presence
 57 of liquid water on the surface of Mars today. These results also suggest that gully land-
 58 forms on other planets can be formed by both sublimation-driven flows and fluid-driven
 59 flows.

60 **1 Introduction**

61 Despite the lack of stable liquid water on Mars today (Hecht, 2002; Richardson &
 62 Mischna, 2005), Mars is a geomorphologically active planet. Numerous studies in the last
 63 decades have documented a range of geomorphic activities (for an overview see (Diniega
 64 et al., 2021)). Among the most active landforms on Mars are Martian gullies (Figure 1).
 65 These landforms consist of an erosional alcove, a channel, and a depositional apron and
 66 resemble debris flow systems on Earth (Malin & Edgett, 2000; Costard et al., 2002; Con-
 67 way et al., 2011; Johnsson et al., 2014; T. de Haas et al., 2015c). Since their discovery,
 68 Martian gullies have been a topic of scientific debate because of the possible link between
 69 their formation and liquid water (Malin & Edgett, 2000; Costard et al., 2002; T. de Haas

et al., 2015c; Dickson et al., 2023), and thus planetary habitability (Hoffman, 2002; Cottingin et al., 2017).

Present-day activity in gullies is observed in subsequent images as new depositional lobes on aprons, the carving of new channels, and the movement of meter-scale boulders (Dundas et al., 2010; Diniega et al., 2010; Dundas et al., 2015; Raack et al., 2020; Sinha & Ray, 2023). As this activity is observed on slopes as low as 10° (Dundas et al., 2019), the material needs to have been fluidized to a certain degree (T. de Haas et al., 2019) and thus dry granular processes cannot have been the cause of the change. In the last decade, the leading hypothesis behind the recent activity in these gullies has shifted from water-driven flows (with or without the involvement of brines) (e.g., Malin & Edgett, 2000; Costard et al., 2002; Knauth & Burt, 2002; Lanza et al., 2010; Levy et al., 2010; Conway et al., 2011; Johnsson et al., 2014; T. de Haas et al., 2015c) to flows driven by the sublimation of CO₂ frost (e.g., Diniega et al., 2010; Dundas et al., 2010, 2012, 2015; Raack et al., 2015, 2020; Pilorget & Forget, 2016; T. de Haas et al., 2019; Khuller et al., 2021; Dundas et al., 2022; Pasquon et al., 2023; Sinha & Ray, 2023). This shift is inspired by the lack of stable water on the Martian surface (Hecht, 2002; Richardson & Mischna, 2005) and a suite of remote sensing studies, showcasing the correlation between the spatial and temporal distribution of gully activity with that of CO₂ frost on the surface of Mars (Diniega et al., 2010; Dundas et al., 2010, 2012, 2015; Raack et al., 2015; Pasquon et al., 2019; Raack et al., 2020; Khuller et al., 2021; Dundas et al., 2022; Pasquon et al., 2023; Sinha & Ray, 2023) (for examples see Figure 1). The CO₂-driven granular flow hypothesis is supported by modelling studies advocating for the possibility of CO₂ gas to fluidize granular material under the thin Martian atmosphere when CO₂ sublimates (Pilorget & Forget, 2016; Cedillo-Flores et al., 2011; T. de Haas et al., 2019). Furthermore, experimental studies have proven that the sublimation of CO₂ ice in the thin Martian atmosphere can destabilize granular materials on slopes (Sylvest et al., 2016, 2019) and even fluidize small volumes of granular material on low angles (Roelofs et al., n.d.). The low atmospheric pressure of the Martian atmosphere is key in this process because of the large gas flux that is created when CO₂ ice sublimates and turns into CO₂ gas (Diniega et al., 2013; Sylvest et al., 2016; T. de Haas et al., 2019; Sylvest et al., 2019; Roelofs et al., n.d.). The gas flux, induced by the sublimation, depends on the ratio between the density of CO₂ ice and gas. In the thin Martian atmosphere (~800 Pa), the gas flux created by CO₂ sublimation is >100 larger than under Earth's atmosphere and thus likely sufficient to fluidize sediments (Cedillo-Flores et al., 2011; T. de Haas et al., 2019).

There are currently two "source-to-sink" hypotheses that attempt to explain how and why CO₂ ice sublimates near granular material on Mars, how this process mobilizes the granular material, and how it transports it over longer distances. The first hypothesis considers a layer of translucent CO₂ ice on top of a layer of regolith (Pilorget & Forget, 2016). This hypothesis is, in essence, the 'Kieffer model' explaining the formation of high-latitude defrosting spots (Kieffer, 2007) on a slope. According to this model, the translucency of CO₂ ice allows the solar radiation at the end of winter to heat up the underlying regolith during the day. This heat causes basal sublimation of the overlaying ice layer, building up the air pressure underneath the ice. This pressure can be large enough to lift the ice layer and eventually break it, forming jets of pressurized CO₂ gas (Hoffman, 2002; Kieffer, 2007). The gas flux created can potentially destabilize large amounts of slope material, also underneath the ice (Pilorget & Forget, 2016). However, the requirement of slab ice means that the latter mechanism is only applicable to Martian gullies at latitudes > 40°S where evidence for slab ice is observed (Dundas et al., 2017, 2019), whereas half of the observed active gully sites on the southern hemisphere are present at latitudes < 40°S (Dundas et al., 2022). Furthermore, this hypothesis does not explain how the pressurized flows underneath a layer of CO₂ ice would result in the deposition of new lobate deposits and the movement of meter-scale boulders.

The second hypothesis explains the observations of fluidized granular flow via two effects within a mix of sediment and CO₂ ice tumbling down a gully (Dundas et al., 2017). The initial mass movement can be triggered by many different processes, unrelated and related to CO₂ ice sublimation, for example, dry raveling, rock fall, marsquakes, meteor impacts or CO₂ sublimation-induced slumping (Sylvest et al., 2016, 2019). In the event that a mixture of CO₂ ice and granular material starts to move, the potential energy of the fall is converted to kinetic energy that must be dissipated as heat or latent heat loss in the form of sublimating CO₂ (Dundas et al., 2017; T. de Haas et al., 2019; Roelofs et al., n.d.). Furthermore, eroded and entrained sediment from the shallow subsurface or unfrosted areas could add additional heat to the mixture, enhancing sublimation (Hoffman, 2002; Dundas et al., 2017). The sublimation of the ice in the sediment-ice mixture is hypothesized to create a gas flux large enough to decrease intergranular friction and fluidize the mixture in such a way that it explains recent flows (T. de Haas et al., 2019; Roelofs et al., n.d.).

Details aside, all current theories on the CO₂-driven fluidization of granular material on Mars agree on two crucial points; (1) heat is needed to sublimate the CO₂, and (2) increased pore pressure, from the CO₂ gas, in the granular material is crucial to decrease intergranular friction and cause fluidisation. However, major research questions remain unanswered. First, it remains speculative whether and exactly how the sublimation of CO₂ ice is able to fluidize granular material. Second, it is unknown how much CO₂ ice needs to sublimate to explain the observed changes. Third, it is unclear how CO₂-driven granular flows on Mars create landforms that are practically identical to landforms created by water-driven debris flows on Earth. Active depositional aprons on both Earth and Mars show lobate deposits with clear levees, and contain meter-scale boulders that are transported through the gully system (T. de Haas et al., 2019; Raack et al., 2020; Dundas et al., 2022). The similarity in key elements in these landforms suggests similarity in the flow dynamics, but this remains unproven.

In this work, we experimentally study the fluidization of granular material by CO₂ ice sublimation under Martian conditions. We aim to (1) resolve the boundary conditions needed to fluidize granular material by CO₂ ice sublimation on Mars, (2) understand the fluid dynamics of CO₂-driven granular flows, and (3) understand the similarities between the CO₂-driven granular flow deposits on Mars and debris-flow deposits on Earth.

To overcome the lack of in-situ observations of CO₂-driven granular flows, we designed two experimental granular flow set-ups that were used to conduct experiments under Martian atmospheric pressure in environmental pressure chambers. In these experiments, granular flows driven by the sublimation of CO₂ in a mixture of sediment and CO₂ ice were created under different boundary conditions, i.e. CO₂ content and slope, and on two different scales to understand potential scale effects. The results of these experiments provide new insights into the flow dynamics of CO₂-driven granular flows on Mars and the resulting deposit morphologies. It is important to note that with our research we specifically aim at studying the transport and deposition processes of CO₂-driven granular flows, rather than the initiation mechanisms behind these flows.

165 **2 Materials and Methods**

166 To study if and how a mixture of CO₂-ice and granular material is fluidized under
 167 Martian atmospheric conditions we designed two experimental set-ups at two different scales based on terrestrial debris flow flumes (Iverson et al., 2010; T. de Haas et
 168 al., 2015b; Roelofs et al., 2022). The flumes were placed in two environmental chambers
 169 of different sizes to enable us to conduct experiments under Martian atmospheric conditions (Figure 2.a–b). Similar to terrestrial debris flow flumes, our flumes consisted of
 170 a steep and narrow chute ending on a larger outflow plain with a lower angle (Figure 2.c–
 171 f). The steep and narrow chute is used to study flow characteristics, e.g. flow depth, ve-
 172 locity, and pore pressures. Whereas the larger plain is used to study deposit morphol-
 173 ogy. The angle of the chute was varied during our experiments, whereas the angle of the
 174 outflow plain was kept constant (Figure 2.e–f). As is common practice in debris flow ex-
 175 periments, we stored the material that makes up the granular flow in a reservoir at the
 176 top of the flume before controlled release. Using flumes of two different sizes enabled us
 177 to study possible scaling issues known to influence the behaviour of experimental ter-
 178 restrial debris flows (Iverson, 2015). The small-scale flume has a total length of 1.80 m
 179 and has a material reservoir that can store between 1.0 and 1.6 kg of material (Figure
 180 2.e). The large-scale flume has a total length of 4.60 m and has a material reservoir that
 181 can store between 8.0 and 11.2 kg of material (Figure 2.f). This means that, while the
 182 large flume is only a factor 2.5 longer than the small flume, the granular flow it supports
 183 is 10 times larger.
 184

186 The small-scale flume was used for conducting experiments in the Mars chamber
 187 of the Hyper Velocity and Impact lab (HVI-lab) at the Open University in Milton Keynes
 188 in the United Kingdom in the autumn of 2021. The large-scale flume was used for con-
 189 ducting experiments in the Mars Simulation Wind Tunnel at Aarhus University in Den-
 190 mark in the autumn of 2022. To compare results between the flumes, experiments were
 191 performed with similar initial and boundary conditions. In this manuscript, 46 exper-
 192 iments conducted in the small-scale set-up in the Mars chamber of the Open University
 193 are presented, and 15 experiments conducted in the large-scale set-up in the Mars Sim-
 194 ulation Wind Tunnel are presented.

195 **2.1 Chamber and flume details**

196 The Mars chamber of the HVI-lab at the Open University is a cylindrical low-pressure
 197 chamber with a length of 2 m and an inner diameter of 0.9 m (Conway et al., 2011; Sylvest
 198 et al., 2016) (Figure 2.a). The chamber can replicate Martian atmospheric conditions
 199 and a range of different temperatures.

200 The Mars Simulation Wind Tunnel at Aarhus University is a cylindrical low-pressure
 201 wind tunnel, originally designed to simulate eolian transport processes on Mars (Holstein-
 202 Rathlou et al., 2014) (Figure 2.b). The chamber has a total length of 8 m and an inner
 203 diameter of 2.15 m. In both chambers, electrical and mechanical feedthroughs exist to
 204 enable the operation of the experimental set-up in the chamber from the outside. Both
 205 chambers have multiple porthole windows that allow for videography of the experiments.

206 Both the large-scale and the small-scale flume were mostly constructed out of Lexan,
 207 a transparent polycarbonate resin thermoplastic, that can deform considerably without
 208 cracking or breaking. The transparency of the Lexan was an important design prereq-
 209 uisite because it allowed us to study the granular flow from the side of the chute. The
 210 bottom of the chute was created out of aluminium, with heating pads installed under-
 211 neath it that controlled the temperature of the chute bottom, which was kept at 20 °C
 212 during the experiments. On the edges of the outflow plain, markers were attached that
 213 were used for creating 3D models of the outflow morphologies using photogrammetry with
 214 Agisoft Metashape software. The outflow plains of the flumes were further covered with
 215 antislip material (3M Safety-Walk 500 series, equal to 80 grit sandpaper with 0.2 mm

216 median sand diameter) to mimic natural roughness. To achieve the same for the chute
 217 bottom, the aluminium was sandblasted. The sediment and ice reservoirs on top of the
 218 flumes were constructed out of copper for the small set-up, and out of aluminium for the
 219 large set-up, because of their relatively low deformation under low temperatures. The
 220 reservoirs in both flumes are opened by means of mechanically operated trap doors. In
 221 the small-scale flume the entire reservoir opened at once, whereas in the large-scale flume,
 222 the opening height was set at 5 cm. This difference in design allowed a more constant
 223 and stable flow of granular material in the large-scale experiments, providing better in-
 224 sight into the flow dynamics.

225 In both flumes, the same sensors were used to study the flow dynamics. In the down-
 226 stream part of the chute, four sensors were installed underneath the chute bottom plate
 227 (Figure 2.e-f); a geophone (Geospace GS-20DX), two relative gas pressure sensors (Hon-
 228 eywell TruStability HSCDRRD006MGAA5), and a load cell (HBM PW6D – 3 kg). The
 229 geophone and the load cell were attached to individual load plates of 5 by 5 cm. The geo-
 230 phone recorded seismic vibrations during the experiment, the pressure sensors recorded
 231 the gas pressure at the bottom of a flow relative to the ambient pressure, and the load
 232 cell recorded the weight of the granular material as the flow passed. Above the flume,
 233 multiple laser distance sensors (Baumer OADM 20U2480/S14C) were installed that recorded
 234 the flow depth at sub-mm accuracy. In the small-scale set-up two laser distance sensors
 235 were used, whereas in the large-scale set-up, four laser distance sensors were used. With
 236 the time difference of the arrival of the flow front at the different laser distance sensors,
 237 reconstructed from the flow depth data, flow velocity was calculated. In both set-ups,
 238 the last laser distance sensor was installed above the load cell (Figure 2e-f). This allowed
 239 us to reconstruct the density of the flow, ρ_m , according to:

$$\rho_m = \frac{M}{AH} \quad (1)$$

240 where M is the mass recorded by the load cell (kg), A is the area of the load cell (m^2),
 241 and H is the flow depth (m). Furthermore, by combining the load cell data and the data
 242 from the pore pressure sensors, the percentage of the material in the flows carried by the
 243 gas pressure could be quantified. The latter is a measure of the degree of fluidisation.
 244 For more detailed photos of the chambers, the flumes and the sensors see Supplemen-
 245 tary Figure 1.

246 The amount of CO_2 ice sublimating during the flow in the large-scale set-up could
 247 be calculated from the data produced by a capacitance pressure sensor in the Mars Sim-
 248 ulation Wind Tunnel. By adding the pressure drawdown caused by the pumping to the
 249 observed pressure increase during the experiment we reconstructed the amount of CO_2
 250 released into the chamber during the flow for three individual experiments with vary-
 251 ing amounts of CO_2 ice in the granular mixture (Figure 7).

252 Multiple video cameras were installed in and around both chambers. For the small-
 253 scale set-up, every experiment was recorded with a Go-Pro camera from the side and a
 254 camcorder from the front. For the large-scale set-up, every experiment was recorded with
 255 two webcams in the chamber that looked at the chute from the side, and one high-speed
 256 camera that filmed the flow at the transition from the chute to the outflow plain at a
 257 frame rate of 600 Hz.

258 2.2 Materials used and experimental routine

259 Two materials form the ingredients of the granular mixture in our experiments; sand
 260 and CO_2 ice. The sand for the experiments is a mixture of fine-grained sand (silver sand
 261 of marine origin, D_{50} of 270 μm) and coarse-grained sand (builders sand of fluvial ori-
 262 gin, D_{50} of 490 μm), combined in a specific ratio (0.6–0.4) to create a broad grain size
 263 distribution (D_{50} of 310 μm , Supplementary Figure 2) that minimizes gas permeability
 264 relative to a mono-disperse sand, and thus slows down the gas escape rate. Experiments

conducted with only silver sand or only builders sand behave similarly overall, although finer mixtures flow further onto the outflow plain. Results of these experiments are presented in the Supplementary Material (see Supplementary Figure 6). The sand was pre-dried in the oven and cleared of any excess moisture in the environmental chambers by putting it in a vacuum prior to the experiments.

The CO₂ ice used for our experiments was ordered in pellet form from commercial parties close to the labs. The CO₂ ice pellets were then crushed to the size of the coarsest sand grains. For the small-scale experiments, this was done by hand with the use of a mortar and pestle. For the large-scale experiments, the ice was crushed with the KitchenAid 5KGM grain mill. Despite the difference in methods, the resulting CO₂ ice grains are similar in size and shape (see Supplementary Figure 3.c-d). To limit the contamination of the CO₂ ice with water, the CO₂ ice was stored in closed polystyrene foam containers in a sealed freezer (Supplementary Figure 3.a-b), and the ice was refreshed at least once a week.

For every experiment, CO₂ ice would be freshly crushed and mixed with a specific amount of sand. To control the amount of CO₂ ice at the start of an experiment, the combined weight was monitored during the mixing process. The loss of CO₂ due to sublimation was compensated by adding more crushed CO₂ ice. Once the desired weight ratio of sediment and CO₂ ice was reached, the mixture was poured into the sediment-ice reservoir in the flume. After this, the chamber was closed and depressurized to an atmospheric pressure of ~8 mbar, a process that took between 12–15 min in the Mars Chamber at the Open University and between 20–25 min in the Mars Simulation Wind Tunnel at Aarhus University. At this pressure, the mixture was released into the flume, while the sensor data was logged and the videos recorded the passing of the granular flow.

2.3 Explored parameter-space

To determine the conditions under which CO₂-driven granular flows can occur on Mars, experiments were conducted under different initial and boundary conditions. For both the experiments in the small-scale and the large-scale set-up, the CO₂-sediment ratio was systematically varied, as well as the slope of the chute. The CO₂-sediment ratio was varied between 0 and 0.6 in the small-scale experiments and varied between 0 and 0.4 for the large-scale experiments (Table 1), while keeping the flume chute at a stable angle of 30°. Note that the mass ratio here is the ratio between the mass of the CO₂ and the sediment before depressurization of the chamber. During depressurization the CO₂ sublimates, which causes the mass ratio to change. We quantified this change for both the small- and large-scale setup by doing initial tests tracking the weight of the mixture inside the sediment-ice reservoir while depressurizing the chamber. The results of these tests can be found in Supplementary Figure 4. In the subsequent sections of this manuscript, we switch from using the initial CO₂-sediment mass ratios to using the mass fraction of CO₂ at the start of an experiment derived from these tests.

Table 1. Parameters explored in the experiments and the tested values. All parameters and values reported in this table are tested in the small-scale setup. The values of the parameters in bold font and teal colour are the ones also tested in the large-scale setup. For more details on the grain-size distributions see Supplementary Figure 2. For a full list of all experiments see Supplementary material.

Variable	Unit	Standard value	Tested values
CO ₂ -sediment ratio	(kg/kg)	0.3	0, 0.1, 0.2, 0.3, 0.4 , 0.5, 0.6
Chute angle	°	30	20, 25, 30
Sediment type		Sand mixture	Sand mixture , Fine, Coarse
Atmospheric pressure	mbar	8	8, 1000

The angle of the chute was varied between 20 and 30 degrees in both the small-scale and the large-scale experiments (Table 1), while keeping the initial CO₂-sediment mass ratio at 0.3. In the small-scale experiments, we did additional tests with different sediment types and under Earth atmospheric pressure (Table 1). To account for the effects of natural variability, each experimental setting was repeated at least twice, and when time allowed three times. A complete list of all experiments and their initial and boundary conditions can be found in the Supplementary material 8.

2.4 Flow characterization

To characterize the dynamics of the CO₂-driven granular flows and objectively compare the flows of different sizes three dimensionless numbers are used; the Bagnold, Savage, and friction numbers. These numbers are used in both debris flow (Iverson, 1997; Iverson & Denlinger, 2001; Roelofs et al., 2022, 2023) and pyroclastic literature (Smith et al., 2020) and therefore also allow for comparison between the CO₂-driven granular flows, and terrestrial debris flows and pyroclastic flows. The numbers describe the relationship between the motion-resisting forces in granular flows; collisional forces, frictional forces, and viscous forces (Iverson, 1997; Parsons et al., 2001; Iverson et al., 2010). The relative importance of these forces plays a big role in both erosional (T. d. de Haas & Woerkom, 2016; Roelofs et al., 2022) and depositional processes (T. de Haas et al., 2015b; Zhou et al., 2019) and is, therefore, an important tool in understanding how certain flows lead to certain morphological features. The Bagnold number describes the ratio between collisional and viscous forces (Iverson, 1997):

$$Nb = \frac{v_s \rho_s \delta^2 \gamma}{v_f \mu} \quad (2)$$

wherein v_s is the volumetric solids fraction, ρ_s is the density of the sediment grains, δ is the D₅₀ grain size of the sediment (m), v_f is the volumetric fluid fraction, μ is the dynamic viscosity of CO₂ gas under Martian atmospheric conditions, which is 9.82*10⁻⁶ Ns/m² (Bardera et al., 2020), and γ is the flow shear rate (1/s):

$$\gamma = \frac{u}{H} \quad (3)$$

wherein u is the flow velocity (m/s). According to Iverson (1997), collisional forces dominate at $N_b > 200$.

The Savage number quantifies the ratio between collisional and frictional forces:

$$Ns = \frac{\rho_s \delta^2 \gamma^2}{(\rho_s - \rho_f) g H \tan \phi} \quad (4)$$

wherein g is the gravitational acceleration (m/s²), ρ_f is the density of the fluid, in our case this is the density of the CO₂ gas at 8 mbar, and ϕ is the internal angle of friction, assumed to be 42° (Parsons et al., 2001; T. de Haas et al., 2015b). The density of the CO₂ gas at a certain pressure can be calculated from the ideal gas law:

$$\rho_f = \frac{PM_m}{RT} \quad (5)$$

wherein P is the atmospheric pressure (Pa), M_m is the molar mass of CO₂, R is the universal gas constant, and T is the temperature (K). For $N_s > 0.1$ collisional forces dominate viscous forces (Iverson, 1997). The friction number is then defined as the Bagnold number divided by the Savage number, describing the ratio between frictional and viscous forces. According to experimental data of wet experimental debris flows of Parsons et al. (2001) and T. de Haas et al. (2015b) frictional forces dominate over viscous forces at $N_f > 100$ for the flow body and $N_f > 250$ for the flow front.

343 **3 Results**

344 **3.1 General flow behaviour and morphology**

345 Increased fluidisation of the material was observed for all experiments under Mar-
 346 tian atmospheric pressures with CO₂ ice in the granular mixture. Compared to refer-
 347 ence experiments without CO₂ ice, these experiments showed >2 times larger flow ve-
 348 locities and run-out, with typical flow velocities of 2 m/s for the small-scale flows and
 349 3 m/s for the large-scale flows. For both the large-scale and the small-scale experiments,
 350 flow depths reached maximum values around 2 cm (Figure 3.a-b), and flow densities around
 351 1000 kg/m³. The relatively small flow depth in the large-scale experiments was caused
 352 by the controlled, and limited, outflow height in this setup. In both set-ups, the flow depth
 353 increased rapidly when the flow front arrived and dissipated more slowly when the tail
 354 passed. In experiments without CO₂, as soon as the flow front arrived at the outflow plain
 355 the flow stopped and the chute backfilled with sediment.

356 Both the small-scale and large-scale CO₂-driven granular flows show multiple surges
 357 (see Figure 3.a-b and the Supplementary videos). For all flows with CO₂ in the mixture,
 358 increased gas pressures were registered at the base of the flow (Figure 3.a-b). This gas
 359 pressure carried between 20–60% of the flow mass, independent of the experimental scale
 360 (Figure 3.c). When analysing the high-speed video of the experiment presented in Fig-
 361 ure 3.a it becomes clear that the velocity of the granular flow is highest in the centre of
 362 the flow and that the flow itself is turbulent (see high-speed video in Supplementary videos).

363 The morphology of the outflow deposits of experiments with CO₂ in the granular
 364 mixture often contain multiple lobes formed by different surges (Figure 4). These lobes
 365 are stacked on top of each other (see for example Figure 4.c,l), and, in some cases, next
 366 to each other (see for example Figure 4.f,k). In both the small-scale and large-scale set-
 367 up levees form in experiments where a second surge of granular material deposits on top
 368 of an earlier surge (see Figure 4.b,f). With increased amount of CO₂ in the granular mix-
 369 ture the material flows further out onto the outflow plain (Figure 4.a–f). Increasing the
 370 chute slope by 5–10° also causes the material to flow further onto the outflow plain (Fig-
 371 ure 4.g–l). In the large-scale experiments, a small increase in slope has a larger effect on
 372 the outflow length than doubling the CO₂ content (Figure 4.d–f and Figure 4.j–l). When
 373 no CO₂ is present in the granular mixture only a small sediment cone forms on the tran-
 374 sition from the chute to the outflow plain.

375 **3.2 Flow velocity, depth, and pore pressure**

376 In the large-scale set-up, flow velocities in the lower half of the chute are constant
 377 (Supplementary Figure 5) and reach values around 3 m/s, independent of the CO₂ frac-
 378 tion (Figure 5.a). In the small-scale set-up, for high CO₂ fractions between 0.14 and 0.3,
 379 flow velocities around 2 m/s are recorded at the end of the chute, whereas for the lower
 380 CO₂ fractions the velocity slowly increases from 1 m/s to 2 m/s with increasing CO₂ frac-
 381 tion. When no CO₂ is present in the granular mixtures, no enhanced fluidisation is ob-
 382 served and the frontal velocity of the material is around 1 m/s in both set-ups. The same
 383 can be stated for granular flows with CO₂ in the mixture released under Earth atmo-
 384 spheric pressure. For both the large-scale and small-scale flows, an increase in the chute
 385 angle, from 20° to 30°, causes a small increase in flow velocity, from 2.2 to 3 m/s (Fig-
 386 ure 5.b).

387 Maximum flow depth increases linearly with CO₂ mass fraction for both set-ups
 388 (Figure 5.c). This relation is steeper for the small-scale set-up. When increasing the chute
 389 angle, maximum flow depth decreases in the large-scale set-up from 22 to 14 mm, while
 390 staying around 15 mm in the small-scale set-up (Figure 5.d). Flow depths are stable in
 391 the lower half of the large-scale flume for all experiments (Supplementary Figure 5). In

392 the small-scale flume, the flow depths are still increasing in the lower half of the flume,
 393 especially when the chute is on the steepest angle.

394 Increased basal pore pressures are observed in all experiments. Basal pore pres-
 395 sures increase with increasing CO₂ mass fraction and decrease with increasing chute slope
 396 (Figure 5.e-f). The differential pressure signal, which is the difference between the am-
 397 bient pressure and the basal pressure, is more scattered for the small-scale experiments.
 398 This is likely caused by the combination of smaller, less stable flows, and a higher amount
 399 of deposition of granular material in the chute during the experiment compared to the
 400 large-scale set-up. Maximum added pressures in the large-scale set-up vary between 0.2
 401 and 0.6 mbar, whereas they vary between 0 and 0.4 for the small-scale set-up.

402 The type of granular material used, either silver sand, builders sand, or the mix-
 403 ture, did not significantly influence the flow dynamics of the flows in the small-scale set-
 404 up (Supplementary Figure 6). Frontal velocities, maximum flow depths, and maximum
 405 basal pressure were the same for all sand types. The type of granular material used did
 406 influence the outflow deposit. CO₂-driven granular flows comprised of finer sands flowed
 407 out further.

408 3.3 Flow density, fluidisation and CO₂ sublimation during the flow

409 The density of the flow is calculated from the weight data from the load cell and
 410 the depth data from the laser distance sensor above the load cell. In addition, the load
 411 cell data and the data from the pore pressure sensors are combined to calculate the per-
 412 centage of the material in the flows carried by the gas pressure. Here, we only present
 413 results from the large-scale experiments, because it was not possible to calculate flow den-
 414 sity and degree of fluidisation for the experiments in the small-scale set-up due to the
 415 deposition of material on the load cell while the granular material was still flowing. Based
 416 on the combined data of the entire flow of all large-scale experiments, summarised in box-
 417 plots in Figure 6.a–b, we can state that our experimental CO₂-driven flows have a den-
 418 sity around 1000 kg/m³. This density is not dependent on the CO₂ fraction (Figure 6.a)
 419 but is slightly dependent on the chute angle (Figure 6.b). If the angle becomes steeper,
 420 the density decreases slightly. The fraction of the flow mass supported by the gas pres-
 421 sure ranges between 0.2–0.3 on average, with a small dependency on CO₂ mass fraction
 422 (Figure 6.c–d). For flows with a higher CO₂ fraction, a slightly higher percentage of the
 423 flow is supported by the gas pressure (Figure 6.c).

424 The data from the capacitance pressure sensor in the chamber of the large-scale
 425 set-up shows that for an experiment with a CO₂ mass of 0.59 kg at the beginning of the
 426 experiment (Supplementary Figure 4), only 42 grams of CO₂ sublimates during the flow
 427 (Figure 7.a). For an experiment with a CO₂ mass of 1.12 kg at the beginning of the ex-
 428 periment (Supplementary Figure 4), only 57 grams of CO₂ sublimates during the flow
 429 (Figure 7.b). For an experiment with a CO₂ mass of 2.13 kg at the beginning of the ex-
 430 periment (Supplementary Figure 4), only 92 grams of CO₂ sublimates during the flow
 431 (Figure 7.c). This means that for all experiments between 0.8–1.3% of the total flow mass
 432 (sand and CO₂ ice), and 0.5–0.9% of the volume (assuming a porosity of 0.4) sublimates.
 433 When normalized for chute length, width, and flow duration, the volume loss is 0.3%–
 434 0.55% per m²/s, and the mass loss is 0.025–0.055 kg/m²/s.

435 3.4 Dimensionless flow characteristics

436 To quantitatively compare the flow dynamics of the large-scale and small-scale gran-
 437 ular flows, we characterized the flows using the dimensionless numbers discussed in the
 438 methods; the Bagnold, Savage, and friction numbers (Figure 8). Furthermore, this di-
 439 mensionless analysis provides the opportunity to place the flow dynamics of the CO₂-
 440 driven granular flows into the context of other granular flows, such as debris flows and

441 pyroclastic flows. In all of our experimental CO₂-driven granular flows, frictional forces
 442 dominated over collisional and viscous forces (Figure 8.c–f). In addition, the Bagnold
 443 numbers of our flows indicate that collisional forces dominated over viscous forces (Fig-
 444 ure 8.a–b). The large-scale flows are relatively more collisional than the small-scale flows
 445 (Figure 8.a–d). Increasing the CO₂ mass fraction in the granular mixture does not have
 446 a large effect on the Bagnold or Savage numbers (Figure 8.a–d) . However, it does af-
 447 fect the relation between frictional and viscous forces, making viscous forces less impor-
 448 tant (Figure 8.e–f). An increase in the angle of the chute results in a larger relative in-
 449 fluence of collisional forces (Figure 8.b,d).

450 4 Discussion

451 4.1 Initial and boundary conditions for CO₂-driven flows

452 Our experiments show that granular material can be fluidized by sublimating CO₂
 453 ice under Martian atmospheric conditions (Figure 3 and Figure 5). This is enabled by
 454 the low Martian atmospheric pressure of around 8 mbar, which makes the gas flux from
 455 sublimation large enough to decrease intergranular friction between the grains and flu-
 456 idize the granular material (Figure 5) (Cedillo-Flores et al., 2011; T. de Haas et al., 2019).
 457 Under terrestrial atmospheric pressure of around 1000 mbar, sublimation of CO₂ ice still
 458 occurs, but the gas flux from the ice into the atmosphere is not large enough to decrease
 459 intergranular friction and fluidize the granular material. From our experiments, it can
 460 be inferred that the fluidisation induced by the sublimation of CO₂ ice grains in a gran-
 461 ular mixture can sustain a stable fluidized flow in a channel, i.e. the flume chute, as long
 462 as CO₂ ice is present and enough energy is available for sublimation. In our experiments,
 463 less than 10% of CO₂ ice in the mixture sublimated while in the chute, implying that
 464 the mixture could have likely flowed in a sustained fluidized way in a confined chute with
 465 a length of ∼10-20 metres.

466 The fluidisation of the material by the sublimation of CO₂ ice in the chute is re-
 467 flected in the enhanced frontal flow velocities and increased basal pressures (Figure 5).
 468 In experiments under Martian atmospheric conditions, where CO₂ ice is present in the
 469 granular mixture, velocities between 2 and 3 m/s are reached, whereas frontal velocities
 470 in experiments without CO₂ ice, or with CO₂ ice under Earth atmospheric pressure, are
 471 only 1 m/s (Figure 5). Furthermore, the pressure data show that the gas pressure car-
 472 rries between 20–60% of the total flow mass in the experiments with CO₂ ice (Figure 3.c
 473 and Figure 6).

474 In the large-scale experiments, stable flow velocities around 3 m/s are reached in
 475 the lower part of the chute for all experiments, even for the experiments with the small-
 476 est amount of CO₂ ice in the mixture. This implies that for all the different CO₂ ice frac-
 477 tions tested, the rate of fluidisation is high and comparable, which is supported by only
 478 small differences in the amount of the flow carried by the pore pressure (Figure 6). There-
 479 fore, we hypothesise that granular material can be fluidized by the sublimation of even
 480 smaller amounts of CO₂ ice than we tested. In the small-scale experiments, we do see
 481 an increase in flow velocity and fluidisation rate for the smallest CO₂ ice fractions (Fig-
 482 ure 5.a), which would imply a higher fluidisation rate for larger CO₂ ice fractions. How-
 483 ever, we hypothesize that this trend is likely caused by the limited length of the chute
 484 compared to the distance over which the flow accelerated, instead of an actual relation
 485 between CO₂ fraction and velocity in our small-scale set-up. The longer chute length in
 486 our large-scale set-up allows the flow to reach a stable state where a balance exists be-
 487 tween CO₂ ice sublimation, the reduction in friction because of the induced gas pressure,
 488 and the remaining friction, as we see in the large-scale set-up.

489 Our experiments also show that CO₂-driven granular flows are fluidized enough to
 490 flow on slopes below the angle of repose. CO₂-driven flows in experiments with chute

angles of 20° still reach velocities 2 times higher than those of dry granular material without CO₂. In addition, the CO₂-driven flows continue to flow over the outflow plain of our set-ups, which have even lower slope angles, 10° and 12° for respectively the large-scale and small-scale set-ups. However, as the flow on these outflow plains is unconfined, the granular material spreads out laterally and ultimately halts (Figure 4). The lateral spreading decreases the flow depth and increases the relative amount of friction the flows have to overcome, both by increasing the area for gas escape and increasing the contact between the flow and the surface. These experimental observations on fluidisation on slopes below the angle of repose are important because they support the hypothesis that CO₂-driven flows on Mars can cause the changes we observe, like new depositional lobes on aprons with slopes as low as 10° to 15° (Diniega et al., 2010; Raack et al., 2020; Sinha & Ray, 2023).

The data from the pressure sensors in the chamber of the large-scale set-up highlight that the mass of CO₂ ice that needs to sublime for the fluidisation process is small. For example, to fluidize 8 kg of sand in our experiments, as little as 43 gram of CO₂ ice needs to sublime, equal to ~0.5% of the volume fraction of the flow (Figure 7). In other words, in our experiments, a mass loss of sublimating CO₂ ice between 0.025–0.055 kg/m²/s is enough to create fluidized granular flows.

4.2 Heat transfer from the environment to the CO₂ ice

Our experiments clearly show that granular material can be fluidized by sublimating small amounts of CO₂ ice, less than 1% of the total flow weight, under Martian atmospheric conditions when sufficient energy is available for CO₂ ice sublimation. However, where that energy is coming from on Mars is debated. According to (Dundas et al., 2017; T. de Haas et al., 2019), this energy could be provided by the release of kinetic energy of a fall or from heat from warmer material in contact with the granular mixture of CO₂ ice and sediment. The sublimating ice would consequently increase pore pressures in the involved granular material, which would cause fluidisation and a two-phase granular flow. If all potential energy of a fall of 300 m, as earlier used by Dundas et al. (2017), would be transferred to heat according to:

$$E_p = mgL \quad (6)$$

with m as the mass of the material falling (kg), g the gravitational acceleration on Mars (3.71 m/s²), and L being the fall height, the total available potential energy, E_{pot} , would equal to 1113 J per kg material. For our flume set-ups, the total potential kinetic energy is smaller, with 16.7 J/kg in the large-scale set-up and 5.9 J/kg for the small-scale set-up. However, the enthalpy of sublimation of CO₂ ice, which is the energy needed for the phase transition from ice to gas, is around 26–28 kJ/mol (Stephenson, 1987; Cedillo-Flores et al., 2011; Shakeel et al., 2018), which is equal to an energy of 590–636 kJ/kg, accounting for the molecular mass of CO₂ of 44.01 g/mol. Therefore, the amount of energy needed to sublime CO₂ is much higher than is released from the complete conversion of potential energy to heat, both in our flumes and on Mars. Therefore, we hypothesize, as Dundas et al. (2017) did earlier, that the heat from the environment, thus from warmer material and surfaces in contact with the flow, is the main driver of sublimation instead of kinetic energy conversion.

Granular material at a slightly higher temperature than the CO₂ frost point could make several thousand J/kg available (Dundas et al., 2017). To put numbers to this, for our flumes the energy available in the aluminium bottom plate to sublime CO₂ ice at the frost point temperature can be calculated as follows:

$$E_t = mc\Delta T \quad (7)$$

with m the mass of the aluminium, c the specific heat (902 J/kgK) and ΔT the temperature difference between the temperature of the chute bottom (20 °C, or 293 K) and the

539 CO₂ frost temperature (−120 °C, or 153 K). For our small-scale flume E_t is 67 kJ, and
 540 for our large-scale flume E_t is 324 kJ. If all this thermal energy is used to sublime CO₂
 541 ice, between 0.51 and 0.54 kg of CO₂ ice could sublime in our large-scale set-up and
 542 between 0.1 and 0.11 kg of CO₂ ice could sublime in our small-scale set-up. The pre-
 543 dicted mass of CO₂ that could sublime as a result of heat energy in our large-scale flume
 544 is similar to the actual observed mass of CO₂ ice that sublimated during the flows (Fig-
 545 ure 7).

546 Equation 7 can also be used to estimate the amount of potential thermal energy
 547 available for sublimation at the bottom of a hypothetical gully on Mars. Taking two gullies
 548 in Hale crater, studied by T. de Haas et al. (2019), as an example; we state that our
 549 hypothetical Martian gully is incised in basaltic bedrock ($c = 600 \text{ J/kg}^\circ\text{C}$, $\rho_{\text{basalt}} = 3000$
 550 kg/m³), has a length of 600 m, a width of 15 m, and in the gully, the upper 1 mm of the
 551 surface regolith is heated up to a temperature of 20 °C, which is realistic for active gullies
 552 according to climate modelling (Roelofs et al., n.d.). In this gully system, the total
 553 potential thermal energy equals 2.27×10^6 kJ. If all this energy is used to sublime CO₂
 554 ice, between 3570 and 3840 kg of CO₂ at frost temperature could be sublimated. Sup-
 555 pose we combine the sublimating ice-to-sediment ratio in our experiments, of 0.5–0.9%,
 556 with this estimated CO₂-ice mass for extrapolation purposes. In that case, we can es-
 557 timate that between $\sim 396000 - \sim 769000$ kg or $\sim 247 - \sim 480 \text{ m}^3$ of unconsolidated granular
 558 material could be fluidized in this Martian gully when enough ice is available. Al-
 559 though this estimate is likely too conservative because it does not account for the weaker
 560 Martian gravity and the possible entrainment of warmer sediment, the prediction matches
 561 the back-calculated flow volumes of 415 and 263 m³ in the smaller gullies in Hale crater
 562 (T. de Haas et al., 2019).

563 In general, our experimental granular flow results on thermal energy, flow volume,
 564 and the necessary mass of CO₂, agree with the back-calculated numbers for actual Mar-
 565 tian flows (T. de Haas et al., 2019). Nonetheless, our predicted E_{thermal} neglects impor-
 566 tant parameters and processes in thermodynamics. In the first place, it assumes that all
 567 heat is converted to energy for sublimation during the flow. This is unlikely because heat
 568 transfer does not happen instantaneously and is dependent on the type of heat trans-
 569 fer, the duration of the potential transfer, and the materials involved. The heat trans-
 570 fer process is further complicated by the newly-found turbulent behaviour of CO₂ driven
 571 flows, the presence of multiple materials, the unknown areas of contact between the cold
 572 ice and the warmer materials, and the possible entrainment of warmer material into the
 573 flow (T. de Haas et al., 2019). Furthermore, for experiments, this E_{thermal} does not ac-
 574 count for the constant heat input into our flume from heating pads installed underneath
 575 the aluminium bottom plate. Despite the still unresolved complications, the predicted
 576 thermal energy is multiple orders of magnitude larger than the potential energy trans-
 577 formed from a fall, both in our flumes as in our hypothetical gullies on Mars. The heat
 578 energy from the environment, either transferred by conduction, radiation, or convection,
 579 is, therefore, more likely to be the cause of the sublimation of the CO₂ ice in CO₂-driven
 580 granular flows on Mars. This implies that CO₂-driven granular flows can only occur in
 581 gullies on Mars at specific locations and during specific periods during the Martian year
 582 when CO₂-ice and warmer regolith simultaneously exist in the gully (Roelofs et al., n.d.).

583 4.3 Flow dynamics and morphology of CO₂ driven Martian flows in (ter- 584 restrial) context

585 To enable a fair comparison between the flows in the two different experimental set-
 586 ups, and compare our CO₂-driven flows with other two-phase granular flows we conducted
 587 dimensionless analysis. This analysis shows that the CO₂-driven flows in our experiments
 588 are supercritical two-phase flows (see Froude numbers in Supplementary Figure 7) in which
 589 frictional forces dominate, and collisional forces are more important than viscous forces
 590 (Figure 8). In experimental and real debris flows, frictional forces typically dominate (Iverson,

591 1997; Iverson & Denlinger, 2001; Roelofs et al., 2022, 2023) (Figure 9). In experimen-
 592 tal dense pyroclastic density currents, frictional forces dominate, and viscous forces seem
 593 to be more important than collisional forces (Smith et al., 2020) (Figure 9). The latter
 594 could stem from the relatively small grain size between 45–90 μm used by (Smith et
 595 al., 2020) in their experiments. As far as we found, for only one natural pyroclastic den-
 596 sity current the dimensionless numbers are known, and for that specific flow, the colli-
 597 sional forces seem to dominate over viscous forces (Rowley et al., 1981; Iverson & Den-
 598 linger, 2001) (Figure 9).

599 Despite the variation between the relative importance of certain forces between py-
 600 roclastic density currents, debris flows and our experimental CO₂-driven granular flows,
 601 these different multi-phase flows show similarity in dynamics, especially considering the
 602 variability within one flow group. The similarity becomes even more evident when com-
 603 paring the dynamics of debris flows, dense pyroclastic density currents, and CO₂-driven
 604 flows with the dynamics of mud flows or natural rock avalanches (Figure 9). For both
 605 natural mud flows and rock avalanches, frictional forces are 10²–10⁶ higher than natu-
 606 ral and experimental debris flows, dense pyroclastic density currents, and our CO₂-driven
 607 granular flows. In addition, in mud flows, the viscous forces become more dominant over
 608 collisional forces than for the other flows, and in rock avalanches, collisional forces be-
 609 come 10³–10⁷ more dominant over viscous forces.

610 The similarity in the relative influence of different forces in the flow between our
 611 CO₂-driven granular flows, and other fluidized multi-phase flows on Earth, is reflected
 612 in the similarity in the morphology of the deposits. The deposits of our experiments are
 613 lobate in shape, often show splitting of lobes, and sometimes have levees, similar to the
 614 hypothesized CO₂-driven granular flow deposits on Mars (Hugenholtz, 2008; Lanza et
 615 al., 2010; Levy et al., 2010; Johnsson et al., 2014; Sinha et al., 2018; Conway et al., 2019).
 616 These morphological elements are also observed in debris flow deposits (Hubert & Fil-
 617 ipov, 1989; Blair & McPherson, 1998; de Haas et al., 2015a, 2018) and pyroclastic flow
 618 deposits (Rowley et al., 1981; Lube et al., 2007; Jessop et al., 2012), whereas they are
 619 less pronounced in mudflow deposits and absent in rock avalanche deposits (Figure 10).
 620 Not all of our outflow deposits contain different distinct lobes or levees, but nor do all
 621 recent deposits in gullies on Mars. A lack of levees might indicate a lack of clear grain
 622 size segregation, which is believed to contribute to levee formation (Jessop et al., 2012;
 623 Johnson et al., 2012; Baker et al., 2016). This could be caused by a more narrow grain
 624 size distribution or a relatively smaller influence of collisional forces over viscous forces.
 625 The latter can stem from a relatively small median grain size or high shear rates (see equa-
 626 tion 2). Another factor that could influence the absence of levees in most of the lobes
 627 in our experimental work is the limited amount of surface friction and the inability of
 628 pore pressures to dissipate into the substrate and for particles to interact with the sub-
 629 strate. Earlier experimental work on terrestrial debris flows has shown that when ex-
 630 perimental debris flows deposit on a layer of permeable sand the formation of levees is pro-
 631 moted (T. de Haas et al., 2015b).

632 4.4 Scaling and upscaling to Mars

633 From experiments with debris flows we know that small-scale flows experience larger
 634 effects of yield strength, viscous flow resistance, and grain inertia than field size flows
 635 (Iverson, 1997; Iverson & Denlinger, 2001; Iverson et al., 2010; Iverson, 2015). In addi-
 636 tion, for small-scale experimental debris flows it has been proposed that they are insuf-
 637 ficiently affected by pore-fluid pressure (Iverson, 1997; Iverson & Denlinger, 2001; Iver-
 638 son et al., 2010). However, certain steps can be, and were, taken to overcome these scal-
 639 ing problems and use small-scale experiments for valid representation of real-world phe-
 640 nomena. For example, when scaling for momentum, a steeper slope in granular flow ex-
 641 periments can induce larger flow velocities to combat the effects of a smaller flow mass.
 642 Furthermore, it is important to evaluate the validity of experimental findings for the nat-

ural world by comparing flow dynamics expressed in dimensionless analysis. From the dimensionless analysis performed and discussed in the section above we can state that our CO₂-driven granular flows behave dynamically similar to debris flows and pyroclastic forms on Earth, both on an experimental and field scale (Figure 9). In addition, our experimental CO₂-driven granular flows show similar flow behaviour to those of back-calculated CO₂ driven flows in Hale crater (T. de Haas et al., 2019), with similar fractions of CO₂ needed for fluidisation, and similar flow velocities around 3 m/s in the steepest parts of the gullies and run-outs on slopes ranging between 13–19°.

The different sizes of the two experimental set-ups allow an assessment of the influence of scaling on CO₂-driven flows. From the dimensionless scaling in Figure 8, we can see that in our large-scale set-up, the collisional forces in the flow are of a higher importance than in the flows in the small-scale set-up. This difference is linked directly to the design of the opening mechanism in the large-scale flume, which limits the flow depth relative to the flow velocity more than in the small-scale flume. Additionally, we see that the friction number of our flows in the large-scale set-up is smaller than those in the small-scale set-up. Although significant differences in the dimensionless numbers between the large- and small-scale flows exist, they are small compared to differences in dimensionless numbers of experimental debris flows in the same flume but of different compositions (Roelofs et al., 2022, 2023) or of experimental pyroclastic density currents in the same flume but for different aeration states (Smith et al., 2020).

To summarize, the flow dynamics and morphology of our experimental CO₂-driven flows are comparable to a variety of natural two-phase flows (Figure 9, Figure 10, and Figure 4) and the influence of scale-effects on our experimental CO₂-driven flows seems to be relatively small. Classical scaling problems in debris flow experiments, related to viscous flow resistance, interstitial fluid, and pore pressures, are of a smaller concern in our CO₂-driven flow experiments because of the scale independence of the CO₂ sublimation process, pore pressure, and flow depth (T. de Haas et al., 2019; Roelofs et al., n.d.), and the low viscosity of the CO₂ gas. Therefore, our findings are of direct relevance to full-scale CO₂-driven flows on Mars.

On Mars the gravitational acceleration is 3.71 m/s², and thus 2.6 times smaller than on Earth. This could possibly influence the flow dynamics of CO₂ driven granular flows. We partly accounted for the smaller gravity on Mars by conducting our experiments on multiple slopes, and therefore studying how the changing gravitational component driving our flows would affect the results. However, the most important driver of CO₂-driven flows is the sublimation of the CO₂ frost, which is independent of gravity. The effect of gravity comes into the equation in the form of the weight of the particles in the flow and the speed with which they fall back to the surface. As earlier described by Roelofs et al. (n.d.), the extent to which the flow is suspended is given by a dimensionless group, which describes the ratio of the Darcy pressure $Hq\nu/\delta^2$ to the weight of the flow $Hg\rho_m$:

$$\frac{Hq\mu}{Hg\rho_m d^2} = \frac{q\mu}{g\rho_m \delta^2}. \quad (8)$$

where q is the volume flux of CO₂ in m/s. Here ρ_m and μ are the same for our experiments and Mars while g is different on Mars, but this can be compensated by increasing the grain diameter δ or decreasing the sublimation flux q .

The equation above implies that under Martian gravity only 0.38 of the volume flux of CO₂ is needed compared to Earth to fluidize a flow or that with the same amount of sublimating CO₂ ice significantly larger grains can be transported on Mars. Practically this means that under Martian gravity, if we were to repeat our large-scale experiments, we would be able to decrease the amount of CO₂ used to fluidize 8 kg of sediment over the length of our flume from 42 to 16 g, equal to a volume fraction of ~0.002. This falls in the volume fraction range, 2×10^{-2} – 2×10^{-5} , predicted to be needed for recent gully flows in Hale crater (T. de Haas et al., 2019). Furthermore, the sustained fluidisation

under varying chute and outflow plain angles gives us the experimental evidence that under a range of gravitational accelerations sublimating CO₂ ice can produce two-phase granular flows.

4.5 Implications for Martian landscape evolution and granular flows in the solar system

From extensive analysis of remote sensing data we know that Martian gullies are active landscape features. Dundas et al. (2019); Pasquon et al. (2019); Dundas et al. (2022); Sinha and Ray (2023) observed erosion and transport of material in gullies, the formation of new terraces and erosion of channel segments, the migration of sinuous curves, channel abandonment, and lobate deposits. Dundas et al. (2019) also observed early stages of gully initiation, suggesting that the processes shaping and changing the gullies today are not merely modifying the pre-existing landforms, but are capable of actively shaping the landscape. Despite these observations, it remains debated what the original formation process of these landforms is. Our experimental results support the hypothesis by Diniega et al. (2010); Dundas et al. (2012, 2015, 2019, 2022) that current activity, by granular flow processes driven by CO₂ sublimation, are actively forming Martian gullies, and are not merely modifying older water-formed features, as suggested by Dickson et al. (2023).

The similarity in flow dynamics and morphology between our experimental CO₂-driven granular flows and natural two-phase granular flows on Earth supports their landscape-changing potential. On Earth, the erodible power of debris flows is suggested to be a primary force in cutting valleys in steep landscapes (Stock & Dietrich, 2003). Although the erodible power of CO₂-driven granular flows has yet to be experimentally explored, the observations of the Martian surface (Dundas et al., 2019, 2022; Sinha & Ray, 2023) and the observed dynamics of the experimental flows leave little doubt that erosion of material by CO₂-driven granular flows is possible. With the current state of remote observations and the lack of detailed in-situ sedimentological and geological investigations, it is impossible to completely rule out a water-driven origin of the Martian gullies. However, we need to be cautious about assuming a water-driven past for the Martian gullies when CO₂-related processes can explain present-day gully activity. As most gullies on Mars were formed during the Amazonian period on Mars, when little to no liquid water could exist on its surface, we deem it likely that the gullies on Mars have been modified and possibly formed by CO₂-related processes for the past 1-3 Ga.

For other planetary bodies in our solar system, our experimental results emphasize that the existence of gully-like landforms is not definite proof of flowing liquids. For example, the observed gully landforms on Vesta (Scully et al., 2015) and Mercury (Rothery et al., 2020) could also have a sublimation-related formation process, especially because of the lack of atmosphere of both bodies. Therefore, our results raise an important question on the use of Earth analogues for planetary science. Earth analogues have been essential in the exploration and understanding of planetary surfaces in our solar systems as well as the potential habitability of these planetary surfaces. Analogue studies are the backbone of our understanding of the processes that shaped the surfaces of rocky planets and bodies throughout our solar system. However, the pitfall of Earth analogue studies is the combined problems of unknown-unknowns and equifinality; the principle describing that different processes can result in the same outcome. Our experimental results could therefore be the start of a fundamental reinterpretation of planetary landforms previously thought to be formed by flowing liquids.

5 Conclusion

We experimentally investigated the feasibility of CO₂-ice sublimation as the driving force in fluidized granular flows on Mars. We conducted 68 experiments under Mar-

743 tian atmospheric conditions in two set-ups on different scales to explore under which bound-
 744 ary and initial conditions granular material can be fluidized by the sublimation of CO₂-
 745 ice.

746 Our experiments show that under Martian atmospheric pressure of 8 mbar, the sub-
 747 limation of small quantities of CO₂-ice, ~0.5% of the total flow volume, can fluidize large
 748 volumes of granular material on a range of different slopes, as long as enough thermal
 749 energy is present to initiate the sublimation of the CO₂-ice. Under Martian atmospheric
 750 pressure, the sublimation of CO₂-ice in a granular mixture increases the pore pressure
 751 within the flow by 0.2–0.6 mbar. This increased pressure carries a significant portion of
 752 the total weight of the flow, between 20–60%, which indicates a decrease in granular fric-
 753 tion between the grains and a high degree of fluidisation of the mixture. The fluidisa-
 754 tion of the material results in large flow velocities that exceed velocities in dry granu-
 755 lar flows by a factor 2–3.

756 Dimensionless analysis of the CO₂-driven flows shows that they are dynamically
 757 similar to debris flows and dense pyroclastic density currents on Earth. The flows are
 758 supercritical and turbulent in behaviour, and frictional forces dominate over collisional
 759 and viscous forces. The similarity in flow dynamics is reflected in the similarity in de-
 760 posit morphology. Our experimental CO₂ driven flows contain morphological elements,
 761 like levees and lobes, that are seen as key characteristics of debris flow and pyroclastic
 762 flow deposits. These features are also observed on the depositional aprons of active gull-
 763 ies on Mars. In addition, our findings on flow dynamics and morphology of CO₂ driven
 764 flows support the hypothesis that CO₂-driven processes are actively modifying and form-
 765 ing Martian gullies today. Therefore, CO₂-driven processes are not merely modifying older
 766 features, but can likely be used to explain the evolution of these landforms on Mars dur-
 767 ing the Amazonian, when little to no liquid water was present on the surface of Mars.

768 Furthermore, our calculations highlight the importance of thermal energy in driv-
 769 ing the sublimation of CO₂-ice that propels the fluidisation of granular material. Direct
 770 thermal energy is a far more effective source of energy for sublimation than the conver-
 771 sion of kinetic and potential energy from a fall to heat. This implies that it is likely that
 772 CO₂-driven granular flows can only occur in gullies on Mars at specific locations and dur-
 773 ing specific periods during the Martian year when CO₂-ice and warmer regolith simul-
 774 taneously exist in the gully.

775 Lastly, our experimental results emphasize that the existence of gully-like landforms
 776 on planetary bodies is not definite proof of flowing liquids. Gully landforms could also
 777 be formed by or at least be altered by sublimation-related processes.

778 6 Open Research

779 For all the experiments presented in this manuscript the data collected by the sen-
 780 sors in the flumes and the DEMs of Difference are available via Yoda (online repository
 781 of Utrecht University). The data and an instruction on how we processed the raw data
 782 can be found under this link: <https://public.yoda.uu.nl/geo/UU01/2T6YAU.html>
 783 DOI: 10.24416/UU01-2T6YAU

784 7 Acknowledgments

785 LR was supported by the Dutch Research Council (NWO) - grant OCENW.KLEIN.495
 786 to TdH. The visits to the labs were funded by Europlanet - project number 20-EPN-015
 787 to TdH, Europlanet - project number 20-EPN-023 to LR, and partly in-kind by the School
 788 of Physical Sciences of the Open University under the leadership of MRP through UK
 789 Space Agency Grant ST/X006549/1. We also acknowledge funding from the CNRS INSU

790 Programme Nationale de Planétologie. SJC is grateful for financial support of the French
791 Space Agency CNES for her HiRISE and CASSIS work.

792 Both the Mars Simulation Wind Tunnel laboratory and she Mars chamber of the
793 HVI-lab at the Open University are members of Europlanet (2024) RI and have received
794 funding from the European Union's Horizon 2020 research and innovation programme
795 under grant agreement No 871149.

796 The authors thank the spacecraft and instrument engineering teams for the suc-
797 cessful completion and operation of CaSSIS. CaSSIS is a project of the University of Bern
798 funded through the Swiss Space Office via ESA's PRODEX programme. The instrument
799 hardware development was also supported by the Italian Space Agency (ASI) (ASI-INAF
800 agreement no. I/018/12/0), INAF/ Astronomical Observatory of Padova, and the Space
801 Research Center (CBK) in Warsaw. Support from SGF (Budapest), the University of
802 Arizona (LPL) and NASA are also gratefully acknowledged.

803 **References**

- Baker, J., Gray, N., & Kokelaar, P. (2016). Particle size-segregation and spontaneous levee formation in geophysical granular flows. *International Journal of Erosion Control Engineering*, 9(4), 174–178. doi: <https://doi.org/10.13101/ijece.9.174>
- Bardera, R., Sor, S., & García-Magariño, A. (2020). Aerodynamics of mars 2020 rover wind sensors. In G. Pezzella & A. Viviani (Eds.), *Mars exploration* (chap. 5). Rijeka: IntechOpen. Retrieved from <https://doi.org/10.5772/intechopen.90912> doi: 10.5772/intechopen.90912
- Blair, T. C., & McPherson, J. G. (1998, 09). Recent debris-flow processes and resultant form and facies of the Dolomite alluvial fan, Owens Valley, California. *Journal of Sedimentary Research*, 68(5), 800-818. Retrieved from <https://doi.org/10.2110/jsr.68.800> doi: 10.2110/jsr.68.800
- Cedillo-Flores, Y., Treiman, A. H., Lasue, J., & Clifford, S. M. (2011). Co₂ gas fluidization in the initiation and formation of martian polar gullies. *Geophysical Research Letters*, 38(21). Retrieved from <https://agupubs.onlinelibrary.wiley.com/doi/abs/10.1029/2011GL049403> doi: <https://doi.org/10.1029/2011GL049403>
- Conway, S. J., de Haas, T., & Harrison, T. N. (2019). Martian gullies: A comprehensive review of observations, mechanisms and insights from earth analogues. *Geological Society, London, Special Publications*, 467(1), 7–66. doi: <https://doi.org/10.1144/SP467.14>
- Conway, S. J., Lamb, M. P., Balme, M. R., Towner, M. C., & Murray, J. B. (2011). Enhanced runout and erosion by overland flow at low pressure and sub-freezing conditions: Experiments and application to mars. *Icarus*, 211(1), 443-457. Retrieved from <https://www.sciencedirect.com/science/article/pii/S0019103510003428> doi: <https://doi.org/10.1016/j.icarus.2010.08.026>
- Costard, F., Forget, F., Mangold, N., & Peulvast, J. P. (2002). Formation of recent martian debris flows by melting of near-surface ground ice at high obliquity. *Science*, 295(5552), 110-113. Retrieved from <https://www.science.org/doi/abs/10.1126/science.1066698> doi: 10.1126/science.1066698
- Cottin, H., Kotler, J. M., Bartik, K., Cleaves, H. J., Cockell, C. S., De Vera, J.-P. P., ... others (2017). Astrobiology and the possibility of life on earth and elsewhere.... *Space Science Reviews*, 209, 1–42. doi: <https://doi.org/10.1007/s11214-015-0196-1>
- de Haas, T., Densmore, A., Stoffel, M., Suwa, H., Imaizumi, F., Ballesteros-Cánovas, J., & Wasklewicz, T. (2018). Avulsions and the spatio-temporal evolution of debris-flow fans. *Earth-Science Reviews*, 177, 53-75. Retrieved from <https://www.sciencedirect.com/science/article/pii/S0012825217302465> doi: <https://doi.org/10.1016/j.earscirev.2017.11.007>
- de Haas, T., Kleinhans, M. G., Carboneau, P. E., Rubensdotter, L., & Hauber, E. (2015a). Surface morphology of fans in the high-arctic periglacial environment of svalbard: Controls and processes. *Earth-Science Reviews*, 146, 163-182. Retrieved from <https://www.sciencedirect.com/science/article/pii/S0012825215000641> doi: <https://doi.org/10.1016/j.earscirev.2015.04.004>
- de Haas, T., Braat, L., Leuven, J. R., Lokhorst, I. R., & Kleinhans, M. G. (2015b). Effects of debris flow composition on runout, depositional mechanisms, and deposit morphology in laboratory experiments. *Journal of Geophysical Research: Earth Surface*, 120(9), 1949–1972.
- de Haas, T., Hauber, E., Conway, S., Van Steijn, H., Johnsson, A., & Kleinhans, M. (2015c). Earth-like aqueous debris-flow activity on mars at high orbital obliquity in the last million years. *Nature Communications*, 6(1), 1–6. doi: <https://doi.org/10.1038/ncomms8543>
- de Haas, T., McArdell, B. W., Conway, S. J., McElwaine, J. N., Kleinhans, M. G., Salese, F., & Grindrod, P. M. (2019). Initiation and flow conditions of contemporary flows in martian gullies. *Journal of Geophys-*

- ical Research: Planets, 124(8), 2246-2271. Retrieved from <https://agupubs.onlinelibrary.wiley.com/doi/abs/10.1029/2018JE005899> doi: <https://doi.org/10.1029/2018JE005899>

de Haas, T. d., & Woerkom, T. v. (2016). Bed scour by debris flows: experimental investigation of effects of debris-flow composition. *Earth Surface Processes and Landforms*, 41(13), 1951–1966. doi: <https://doi.org/10.1002/esp.3963>

Dickson, J. L., Palumbo, A. M., Head, J. W., Kerber, L., Fassett, C. I., & Kreslavsky, M. A. (2023). Gullies on mars could have formed by melting of water ice during periods of high obliquity. *Science*, 380(6652), 1363-1367. Retrieved from <https://www.science.org/doi/abs/10.1126/science.abk2464> doi: [10.1126/science.abk2464](https://doi.org/10.1126/science.abk2464)

Diniega, S., Bramson, A. M., Buratti, B., Buhler, P., Burr, D. M., Chojnacki, M., ... Widmer, J. M. (2021). Modern mars' geomorphological activity, driven by wind, frost, and gravity. *Geomorphology*, 380, 107627. Retrieved from <https://www.sciencedirect.com/science/article/pii/S0169555X21000350> doi: <https://doi.org/10.1016/j.geomorph.2021.107627>

Diniega, S., Byrne, S., Bridges, N. T., Dundas, C. M., & McEwen, A. S. (2010, 11). Seasonality of present-day Martian dune-gully activity. *Geology*, 38(11), 1047-1050. Retrieved from <https://doi.org/10.1130/G31287.1> doi: [10.1130/G31287.1](https://doi.org/10.1130/G31287.1)

Diniega, S., Hansen, C., McElwaine, J., Hugenholtz, C., Dundas, C., McEwen, A., & Bourke, M. (2013). A new dry hypothesis for the formation of martian linear gullies. *Icarus*, 225(1), 526-537. Retrieved from <https://www.sciencedirect.com/science/article/pii/S0019103513001668> doi: <https://doi.org/10.1016/j.icarus.2013.04.006>

Dundas, C. M., Conway, S. J., & Cushing, G. E. (2022). Martian gully activity and the gully sediment transport system. *Icarus*, 115133. Retrieved from <https://www.sciencedirect.com/science/article/pii/S0019103522002408> doi: <https://doi.org/10.1016/j.icarus.2022.115133>

Dundas, C. M., Diniega, S., Hansen, C. J., Byrne, S., & McEwen, A. S. (2012). Seasonal activity and morphological changes in martian gullies. *Icarus*, 220(1), 124-143. Retrieved from <https://www.sciencedirect.com/science/article/pii/S0019103512001340> doi: <https://doi.org/10.1016/j.icarus.2012.04.005>

Dundas, C. M., Diniega, S., & McEwen, A. S. (2015). Long-term monitoring of martian gully formation and evolution with mro/hirise. *Icarus*, 251, 244-263. Retrieved from <https://www.sciencedirect.com/science/article/pii/S0019103514002668> (Dynamic Mars) doi: <https://doi.org/10.1016/j.icarus.2014.05.013>

Dundas, C. M., McEwen, A. S., Diniega, S., Byrne, S., & Martinez-Alonso, S. (2010). New and recent gully activity on mars as seen by hirise. *Geophysical Research Letters*, 37(7). Retrieved from <https://agupubs.onlinelibrary.wiley.com/doi/abs/10.1029/2009GL041351> doi: <https://doi.org/10.1029/2009GL041351>

Dundas, C. M., McEwen, A. S., Diniega, S., Hansen, C. J., Byrne, S., & McElwaine, J. N. (2017). The formation of gullies on mars today. *Geological Society, London, Special Publications*, 467(1), 67-94. Retrieved from <https://sp.lyellcollection.org/content/467/1/67> doi: [10.1144/SP467.5](https://doi.org/10.1144/SP467.5)

Dundas, C. M., McEwen, A. S., Diniega, S., Hansen, C. J., Byrne, S., & McElwaine, J. N. (2019). scho. *Geological Society, London, Special Publications*, 467(1), 67-94. Retrieved from <https://sp.lyellcollection.org/content/467/1/67> doi: [10.1144/SP467.5](https://doi.org/10.1144/SP467.5)

Hecht, M. H. (2002). Metastability of liquid water on mars. *Icarus*, 156(2), 373-386. Retrieved from <https://www.sciencedirect.com/science/article/pii/S0019103501967946> doi: <https://doi.org/10.1006/icar.2001.6794>

- 913 Hoffman, N. (2002). Active polar gullies on mars and the role of carbon dioxide. *Astrobiology*, 2(3), 313–323. doi: <https://doi.org/10.1089/153110702762027899>
- 914 Holstein-Rathlou, C., Merrison, J., Iversen, J. J., Jakobsen, A. B., Nicolajsen, R.,
915 Nørnberg, P., ... Portyankina, G. (2014). An environmental wind tunnel
916 facility for testing meteorological sensor systems. *Journal of Atmospheric and
917 Oceanic Technology*, 31(2), 447 - 457. Retrieved from https://journals.ametsoc.org/view/journals/atot/31/2/jtech-d-13-00141_1.xml doi:
918 <https://doi.org/10.1175/JTECH-D-13-00141.1>
- 919 Hubert, J. F., & Filipov, A. J. (1989). Debris-flow deposits in alluvial fans on the
920 west flank of the white mountains, owens valley, california, u.s.a. *Sedimentary
921 Geology*, 61(3), 177-205. Retrieved from <https://www.sciencedirect.com/science/article/pii/0037073889900572> doi: [https://doi.org/10.1016/0037-0738\(89\)90057-2](https://doi.org/10.1016/0037-0738(89)90057-2)
- 922 Hugenholtz, C. H. (2008). Frosted granular flow: A new hypothesis for mass
923 wasting in martian gullies. *Icarus*, 197(1), 65-72. Retrieved from <https://www.sciencedirect.com/science/article/pii/S0019103508001796> doi:
924 <https://doi.org/10.1016/j.icarus.2008.04.010>
- 925 Iverson, R. M. (1997). The physics of debris flows. *Reviews of geophysics*, 35(3),
926 245–296.
- 927 Iverson, R. M. (2015). Scaling and design of landslide and debris-flow experiments.
928 *Geomorphology*, 244, 9-20. Retrieved from <https://www.sciencedirect.com/science/article/pii/S0169555X15001336> (Laboratory Experiments in
929 Geomorphology 46th Annual Binghamton Geomorphology Symposium 18-20
September 2015) doi: <https://doi.org/10.1016/j.geomorph.2015.02.033>
- 930 Iverson, R. M., & Denlinger, R. P. (2001). Flow of variably fluidized granular masses
931 across three-dimensional terrain: 1. coulomb mixture theory. *Journal of Geo-
932 physical Research: Solid Earth*, 106(B1), 537–552.
- 933 Iverson, R. M., Logan, M., LaHusen, R. G., & Berti, M. (2010). The perfect de-
934 bris flow? Aggregated results from 28 large-scale experiments. *Journal of Ge-
935ophysical Research: Earth Surface*, 115(F3). doi: <https://doi.org/10.1029/2009JF001514>
- 936 Jessop, D., Kelfoun, K., Labazuy, P., Mangeney, A., Roche, O., Tillier, J.-L., ...
937 Thibault, G. (2012). Lidar derived morphology of the 1993 lascar pyroclastic
938 flow deposits, and implication for flow dynamics and rheology. *Journal of Vol-
939 canology and Geothermal Research*, 245-246, 81-97. Retrieved from <https://www.sciencedirect.com/science/article/pii/S0377027312002041> doi:
940 <https://doi.org/10.1016/j.jvolgeores.2012.06.030>
- 941 Johnson, C. G., Kokelaar, B. P., Iverson, R. M., Logan, M., LaHusen, R. G., &
942 Gray, J. M. N. T. (2012). Grain-size segregation and levee formation in geo-
943 physical mass flows. *Journal of Geophysical Research: Earth Surface*, 117(F1).
944 Retrieved from <https://agupubs.onlinelibrary.wiley.com/doi/abs/10.1029/2011JF002185> doi: <https://doi.org/10.1029/2011JF002185>
- 945 Johnsson, A., Reiss, D., Hauber, E., Hiesinger, H., & Zanetti, M. (2014). Evi-
946 dence for very recent melt-water and debris flow activity in gullies in a young
947 mid-latitude crater on mars. *Icarus*, 235, 37-54. Retrieved from <https://www.sciencedirect.com/science/article/pii/S0019103514001225> doi:
948 <https://doi.org/10.1016/j.icarus.2014.03.005>
- 949 Khuller, A. R., Christensen, P. R., Harrison, T. N., & Diniega, S. (2021). The distri-
950 bution of frosts on mars: Links to present-day gully activity. *Journal of Geo-
951 physical Research: Planets*, 126(3), e2020JE006577. Retrieved from <https://agupubs.onlinelibrary.wiley.com/doi/abs/10.1029/2020JE006577>
952 (e2020JE006577 2020JE006577) doi: <https://doi.org/10.1029/2020JE006577>
- 953 Kieffer, H. H. (2007). Cold jets in the martian polar caps. *Journal of Geo-
954 physical Research: Planets*, 112(E8). Retrieved from <https://agupubs.onlinelibrary.wiley.com/doi/abs/10.1029/2006JE002816> doi:
955

- 968 https://doi.org/10.1029/2006JE002816
- 969 Knauth, L., & Burt, D. M. (2002). Eutectic brines on mars: Origin and pos-
970 sible relation to young seepage features. *Icarus*, 158(1), 267-271. Re-
971 trieval from <https://www.sciencedirect.com/science/article/pii/S0019103502968661> doi: <https://doi.org/10.1006/icar.2002.6866>
- 972 Lanza, N., Meyer, G., Okubo, C., Newsom, H., & Wiens, R. (2010). Evidence for de-
973 bris flow gully formation initiated by shallow subsurface water on mars. *Icarus*,
974 205(1), 103-112. Retrieved from <https://www.sciencedirect.com/science/article/pii/S001910350900164X> (MRO/HiRISE Studies of Mars) doi:
975 <https://doi.org/10.1016/j.icarus.2009.04.014>
- 976 Levy, J., Head, J., Dickson, J., Fassett, C., Morgan, G., & Schon, S. (2010). Iden-
977 tification of gully debris flow deposits in protonilus mensae, mars: Char-
978 acterization of a water-bearing, energetic gully-forming process. *Earth
979 and Planetary Science Letters*, 294(3), 368-377. Retrieved from <https://www.sciencedirect.com/science/article/pii/S0012821X09004580> (Mars
980 Express after 6 Years in Orbit: Mars Geology from Three-Dimensional Map-
981 ping by the High Resolution Stereo Camera (HRSC) Experiment) doi:
982 <https://doi.org/10.1016/j.epsl.2009.08.002>
- 983 Lube, G., Cronin, S. J., Platz, T., Freundt, A., Procter, J. N., Henderson, C., &
984 Sheridan, M. F. (2007). Flow and deposition of pyroclastic granular flows: A
985 type example from the 1975 ngauruhoe eruption, new zealand. *Journal of Vol-
986 canology and Geothermal Research*, 161(3), 165-186. Retrieved from <https://www.sciencedirect.com/science/article/pii/S0377027306004239> doi:
987 <https://doi.org/10.1016/j.jvolgeores.2006.12.003>
- 988 Malin, M. C., & Edgett, K. S. (2000). Evidence for recent groundwater seepage
989 and surface runoff on mars. *Science*, 288(5475), 2330-2335. Retrieved from
990 <https://www.science.org/doi/abs/10.1126/science.288.5475.2330> doi:
991 <https://doi.org/10.1126/science.288.5475.2330>
- 992 Parsons, J. D., Whipple, K. X., & Simoni, A. (2001). Experimental study of the
993 grain-flow, fluid-mud transition in debris flows. *The Journal of Geology*,
994 109(4), 427-447.
- 995 Pasquon, K., Conway, S., Vincendon, M., Massé, M., Raack, J., Noblet, A., ...
996 Lewis, S. R. (2023). Insights into the interaction between defrosting sea-
997 sonal ices and gully activity from cassis and hirise observations in sisyphe cavi,
998 mars. *Planetary and Space Science*, 235, 105743. Retrieved from <https://www.sciencedirect.com/science/article/pii/S0032063323001125> doi:
999 <https://doi.org/10.1016/j.pss.2023.105743>
- 1000 Pasquon, K., Gargani, J., Massé, M., Vincendon, M., Conway, S. J., Séjourné, A., ...
1001 Lewis, S. R. (2019). Present-day development of gully-channel sinu-
1002 osity by carbon dioxide gas supported flows on mars. *Icarus*, 329, 296-313.
1003 Retrieved from <https://www.sciencedirect.com/science/article/pii/S0019103518304627> doi: <https://doi.org/10.1016/j.icarus.2019.03.034>
- 1004 Pilorget, C., & Forget, F. (2016). Formation of gullies on mars by debris flows trig-
1005 gered by co2 sublimation. *Nature Geoscience*, 9(1), 65-69. Retrieved from
1006 <https://doi.org/10.1038/ngeo2619> doi: 10.1038/ngeo2619
- 1007 Raack, J., Conway, S. J., Heyer, T., Bickel, V. T., Philippe, M., Hiesinger, H., ...
1008 Massé, M. (2020). Present-day gully activity in sisyphe cavi, mars – flow-like
1009 features and block movements. *Icarus*, 350, 113899. Retrieved from <https://www.sciencedirect.com/science/article/pii/S0019103520302785> doi:
1010 <https://doi.org/10.1016/j.icarus.2020.113899>
- 1011 Raack, J., Reiss, D., Appéré, T., Vincendon, M., Ruesch, O., & Hiesinger, H. (2015).
1012 Present-day seasonal gully activity in a south polar pit (sisyphe cavi) on mars.
1013 *Icarus*, 251, 226-243. Retrieved from <https://www.sciencedirect.com/science/article/pii/S0019103514001663> (Dynamic Mars) doi:
1014 <https://doi.org/10.1016/j.icarus.2014.03.040>

- 1023 Richardson, M. I., & Mischna, M. A. (2005). Long-term evolution of transient
 1024 liquid water on mars. *Journal of Geophysical Research: Planets*, 110(E3).
 1025 Retrieved from <https://agupubs.onlinelibrary.wiley.com/doi/abs/10.1029/2004JE002367> doi: <https://doi.org/10.1029/2004JE002367>
- 1026 Roelofs, L., Colucci, P., & Haas, T. d. (2022). How debris-flow composition affects
 1027 bed erosion quantity and mechanisms - an experimental assessment. *Earth
 1028 Surface Processes and Landforms*.
- 1029 Roelofs, L., Conway, S. J., de Haas, T., Dundas, C., Lewis, S. R., McElwaine, J., ...
 1030 Patel, M. R. (n.d.). How, where, and when CO₂ drives current mass flows in
 1031 martian gullies. *In Press at Communications Earth and Environment*.
- 1032 Roelofs, L., Nota, E. W., Flipsen, T. C. W., Colucci, P., & de Haas, T. (2023).
 1033 How bed composition affects erosion by debris flows—an experimental assess-
 1034 ment. *Geophysical Research Letters*, 50(14), e2023GL103294. Retrieved
 1035 from <https://agupubs.onlinelibrary.wiley.com/doi/abs/10.1029/2023GL103294> (e2023GL103294 2023GL103294) doi: <https://doi.org/10.1029/2023GL103294>
- 1036 Rothery, D. A., Massironi, M., Alemanno, G., Barraud, O., Besse, S., Bott, N.,
 1037 ... others (2020). Rationale for bepicolombo studies of mercury's sur-
 1038 face and composition. *Space science reviews*, 216(4), 1–46. Retrieved from
 1039 <https://link.springer.com/article/10.1007/s11214-020-00694-7> doi:
 1040 <https://doi.org/10.1007/s11214-020-00694-7>
- 1041 Rowley, P. D., Kuntz, M. A., & Macleod, N. S. (1981). Pyroclastic-flow deposits. In
 1042 *The 1980 eruptions of mount st. helens, washington* (p. 489–512). Washington:
 1043 USGS. doi: 10.3133/pp1250
- 1044 Scully, J. E., Russell, C. T., Yin, A., Jaumann, R., Carey, E., Castillo-Rogez, J.,
 1045 ... Le Corre, L. (2015). Geomorphological evidence for transient water
 1046 flow on vesta. *Earth and Planetary Science Letters*, 411, 151–163. Retrieved
 1047 from <https://www.sciencedirect.com/science/article/pii/S0012821X14007572> doi: <https://doi.org/10.1016/j.epsl.2014.12.004>
- 1048 Shakeel, H., Wei, H., & Pomeroy, J. (2018). Measurements of enthalpy of sublima-
 1049 tion of ne, n₂, o₂, ar, co₂, kr, xe, and h₂o using a double paddle oscillator. *The
 1050 Journal of Chemical Thermodynamics*, 118, 127–138. Retrieved from <https://www.sciencedirect.com/science/article/pii/S0021961417303968> doi:
 1051 <https://doi.org/10.1016/j.jct.2017.11.004>
- 1052 Sinha, R. K., & Ray, D. (2023). Morphological changes currently occurring
 1053 in sand-filled gully channels on mars: Implications for the role of sub-
 1054 strates inside channels. *Icarus*, 390, 115334. Retrieved from <https://www.sciencedirect.com/science/article/pii/S0019103522004262> doi:
 1055 <https://doi.org/10.1016/j.icarus.2022.115334>
- 1056 Sinha, R. K., Vijayan, S., Shukla, A. D., Das, P., & Bhattacharya, F. (2018). Gullies
 1057 and debris-flows in ladakh himalaya, india: a potential martian analogue. *Geo-
 1058 logical Society, London, Special Publications*, 467(1), 315–342. doi: <https://doi.org/10.1144/SP467.9>
- 1059 Smith, G., Rowley, P., Williams, R., Giordano, G., Trolese, M., Silleni, A., ...
 1060 Capon, S. (2020). A bedform phase diagram for dense granular cur-
 1061 rents. *Nature communications*, 11(1), 2873. doi: <https://doi.org/10.1038/s41467-020-16657-z>
- 1062 Stephenson, R. M. (1987). *Handbook of the thermodynamics of organic compounds*.
 1063 Elsevier. doi: <https://doi.org/10.1007/978-94-009-3173-2>
- 1064 Stock, J. D., & Dietrich, W. E. (2003). Valley incision by debris flows: Evidence of a
 1065 topographic signature. *Water Resources Research*, 39(4). doi: <https://doi.org/10.1029/2001WR001057>
- 1066 Sylvester, M. E., Conway, S. J., Patel, M. R., Dixon, J. C., & Barnes, A. (2016). Mass
 1067 wasting triggered by seasonal co₂ sublimation under martian atmospheric con-
 1068 ditions: Laboratory experiments. *Geophysical Research Letters*, 43(24), 12,363–
 1069
- 1070
- 1071
- 1072
- 1073
- 1074
- 1075
- 1076
- 1077

- 1078 12,370. Retrieved from <https://agupubs.onlinelibrary.wiley.com/doi/abs/10.1002/2016GL071022> doi: <https://doi.org/10.1002/2016GL071022>
- 1079
1080 Sylvest, M. E., Dixon, J. C., Conway, S. J., Patel, M. R., McElwaine, J. N., Hager-
1081 mann, A., & Barnes, A. (2019). Co₂ sublimation in martian gullies: labo-
1082 ratory experiments at varied slope angle and regolith grain sizes. *Geologi-*
1083 *cal Society, London, Special Publications*, 467(1), 343–371. Retrieved from
1084 <https://www.lyellcollection.org/doi/full/10.1144/SP467.11> doi:
1085 <https://doi.org/10.1144/SP467.11>
- 1086 Zhou, G. G., Li, S., Song, D., Choi, C. E., & Chen, X. (2019). Depositional mecha-
1087 nisms and morphology of debris flow: physical modelling. *Landslides*, 16, 315–
1088 332. doi: <https://doi.org/10.1007/s10346-018-1095-9>

Figure 1. Three examples of Martian gullies with frost; a) gullies in Sisyphi Cavi (synthetic RGB CaSSIS images using the PAN and BLU channels, where defrosted surfaces appear red and frosted surfaces white, MY34_003464_256_1, Ls 242°) (Pasquon et al., 2023), b) gullies in an unnamed crater (HiRISE image, ESP_039114_1115, Ls 243°), c) gullies on Matara crater dune field (HiRISE image, ESP_063824_1340, Ls 160°). Colour strips in panels b) and c) are false colours, composed of near-infrared, red and blue-green wavelength signals.

Figure 2. Photos and schematic drawings of chambers (a-b) and flumes (c-f). The photo in panel (a) depicts the Mars chamber at the Hyper Velocity and Impact lab (HVI) of the Open University (UK), panel (b) shows the Mars Simulation Wind tunnel at Aarhus University (Denmark). Details of the small-scale flume set-up used in the Mars chamber of the HVI lab can be found in (c) and (e). Details of the large-scale set-up used in the Mars Simulation Wind tunnel in Aarhus can be found in (d) and (f). All dimensions are given in cm.

Figure 3. Example of flow depth, flow mass, and differential pore pressures (sensors 1 and 2) during an experiment for the large-scale set-up (a) and the small-scale set-up (b) with similar boundary conditions; initial CO₂ mass fraction of 0.23 and flume angle of 20°. The lower panel (c), depicts the mass fraction of the flow carried by the gas pressure for the experiments depicted in panels (a) and (b). As the data from the two pore pressure sensors slightly differs, this fraction is depicted as an envelope covering the range provided by the two sensors. The fraction carried by the gas pressure is a measure for the degree of fluidisation.

Figure 4. Digital elevation models (DEMs) for the outflow deposits of 12 experiments under Martian atmospheric pressures, 6 conducted in the large scale set-up, highlighted by thick black borders, and 6 conducted in the small scale set-up. The top two rows (a–f) show deposits of experiments with varying CO₂ mass fractions. The fractions depicted in the panels correspond to the mass fractions at the start of an experiment derived from Supplementary Figure 4. The bottom two rows (g–l) show deposits of experiments with different chute angles. For all depicted experiments, videos are present in the Supplementary material 8.

Figure 5. Frontal flow velocity (a-b), maximum flow depth (c-d), and maximum differential pore pressure for pore pressure sensor 1 (P1) and pore pressure sensor 2 (P2) (e-f), for the large-scale (L) and small-scale (S) experimental flows. All green and blue dots represent results from experiments conducted under Martian atmospheric pressure, whereas the yellow dots represent results from experiments conducted under Earth atmospheric pressure. The results of experiments with varying CO₂ mass fractions in the flow, but a constant chute angle of 30°, are presented in the left column. Note that the mass fractions presented here are the mass fractions at the start of an experiment derived from data presented in Supplementary Figure 4. The results of experiments conducted under different chute angles, but with a constant initial CO₂ mass fraction of 0.33, are presented in the right column.

Figure 6. Boxplots showing the distribution of the flow density (a-b) and the fraction of the flow carried by the gas pressure (c-d) for the large-scale experiments conducted with different CO₂ mass fractions (left column) and under different chute angles (right column). The data in a single boxplot combines the density or fraction carried by the gas pressure of the main flow over time (flow tails are disregarded) for all large-scale experiments performed under similar conditions (i.e. similar CO₂ mass fractions and chute angle). The dark blue dots represent the mean value during one experiment. The reported p-value in the subplots stems from an ANOVA test of these means. The p-values show that the results from the different experimental groups in panels (b) and (c) are marginally significant.

Figure 7. Flow depth and cumulative CO₂ mass loss for three experiments in the large-scale set-up, with a CO₂ mass at the beginning of the experiment of 0.59 kg (a), 1.12 kg (b), and 2.13 kg (c). All experiments were conducted under a chute slope of 30°. The cumulative CO₂ mass lost is determined based on data from a capacitance pressure sensor in the chamber, the measurement frequency is 1 Hz.

Figure 8. Bagnold (a-b), Savage (c-d), and friction (e-f) numbers for the granular flows in the large-scale and small-scale experiments conducted with different CO₂ mass fractions (left column) and under different chute angles (right column). The horizontal lines indicate the transition from one flow regime to the other (Iverson, 1997). For the Bagnold number (a-b), this is the transition between the collisional and the viscous flow regime. For the Savage number (c-d), this is the transition from the collisional to the frictional flow regime. For the friction number (e-f), this is the transition from the frictional to the viscous flow regime, the latter is not visible in the plot because the flows are far into the frictional flow regime.

Figure 9. Bagnold numbers plotted against Savage numbers for the experimental CO₂-driven flows presented in Figure 4, the experimental debris flows from Roelofs et al. (2022)², the experimental dense pyroclastic density currents from Smith et al. (2020)³, three prototype natural debris flows from Iverson (1997)⁴ and Iverson and Denlinger (2001)⁵, a natural mud flow from Iverson (1997)⁴, a rock avalanche from Iverson and Denlinger (2001)⁵, and a pyroclastic density current from Mount St Helens from Iverson and Denlinger (2001)⁵ and Rowley et al. (1981)⁶

Figure 10. Different natural granular flows and their key morphological features. (a) Debris flow fan with different lobate deposits with levees near Pinnisalm, Neustift im Stubaital, Austria. (b) Pyroclastic density current deposits from the eruption of Mount St Helens in 1980 on July 22, showing multiple channels with levees and lobes (Photo: Dan Miller and USGS, first published in Baker et al. (2016)). (c) Granular flow deposits on the slopes of Istok crater on Mars with levees and lobes (Photo: NASA - HiRISE PSP_006837_1345) (Johnsson et al., 2014; T. de Haas et al., 2015c) (d) Rock avalanche Hope Slide, Hope, British Columbia, Canada (Photo: John Clague). (e) Mud flow dominated Coldwater Canyon fan, California, USA, showing channels and dispersed lobes with thin levees.

Figure 1.

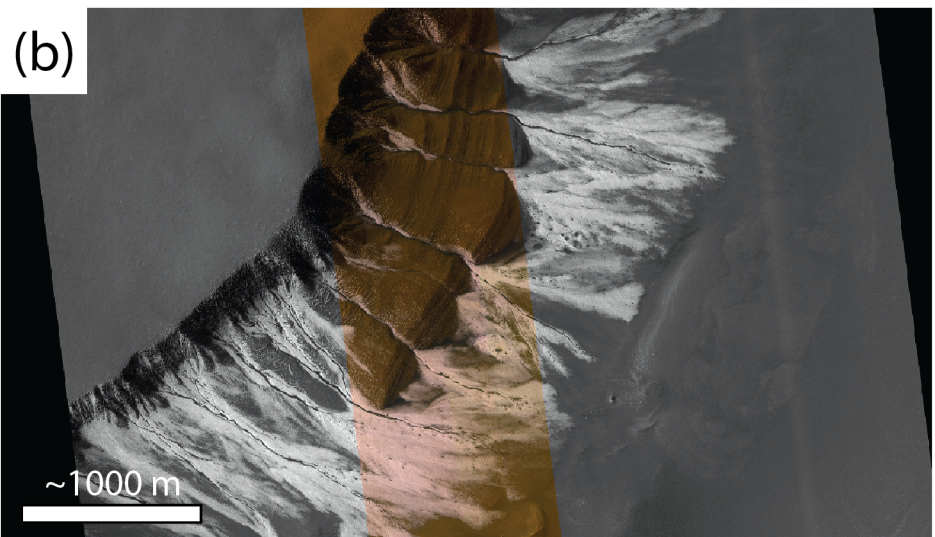
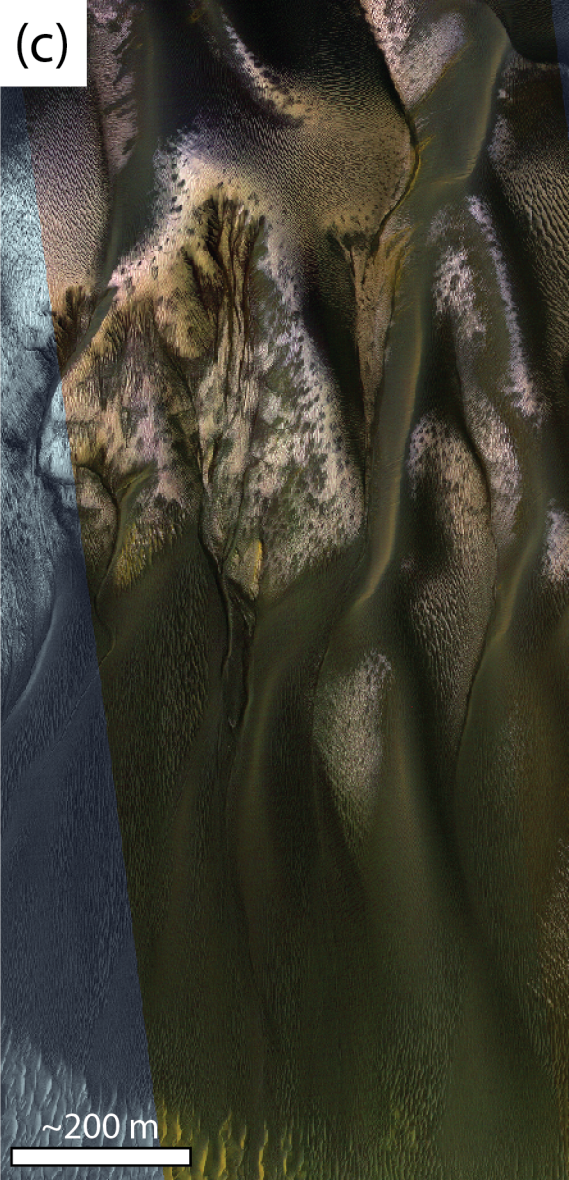
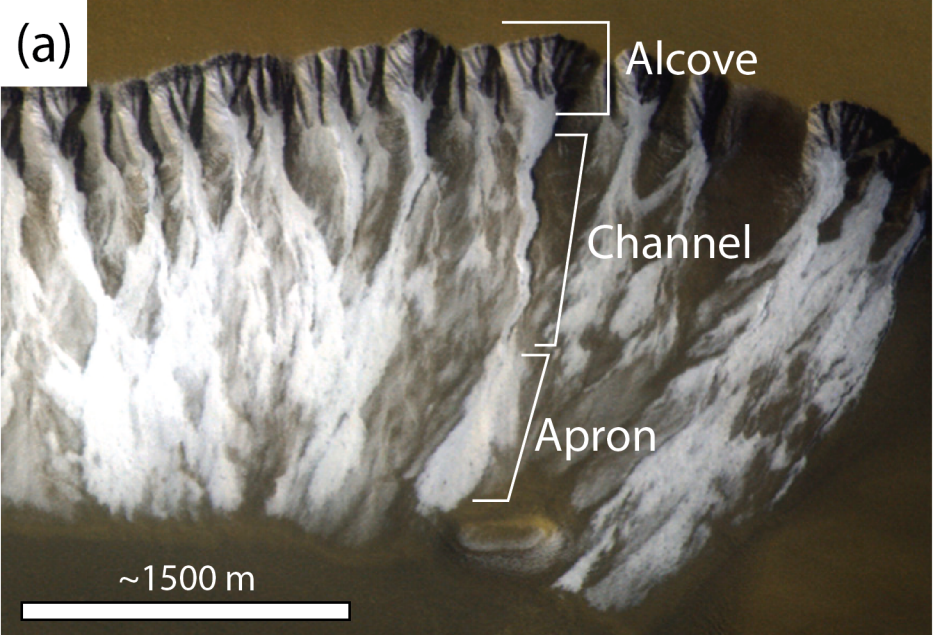


Figure 2.

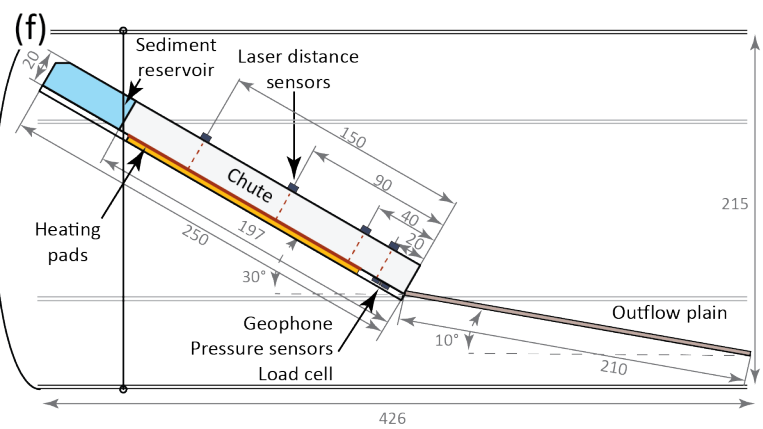
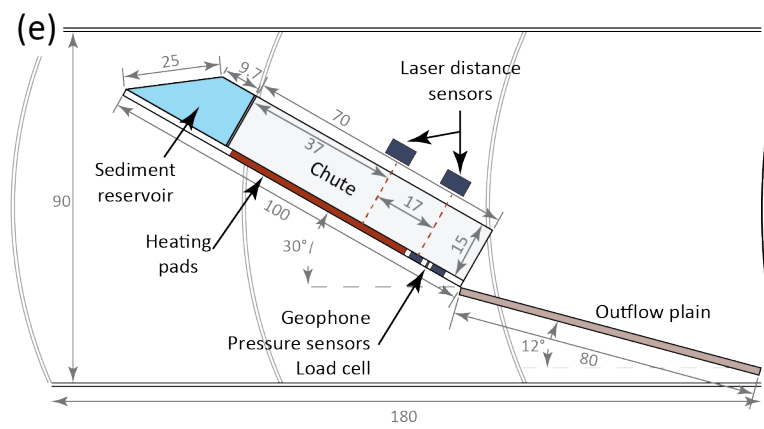
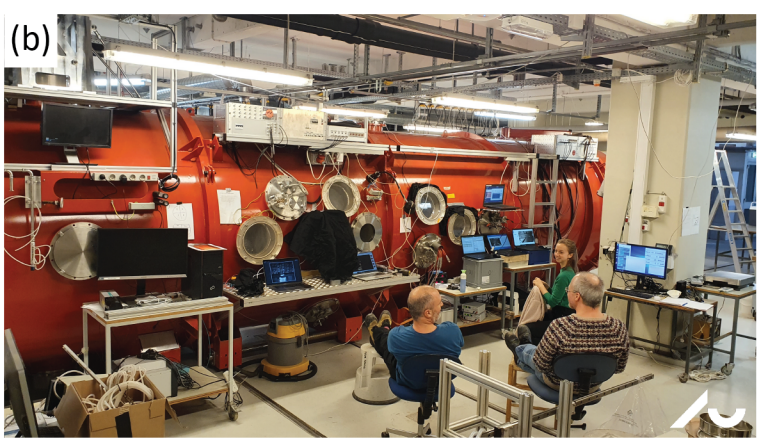
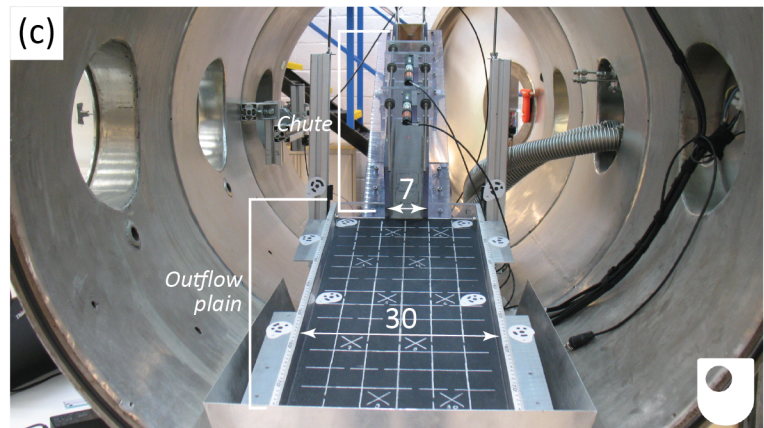
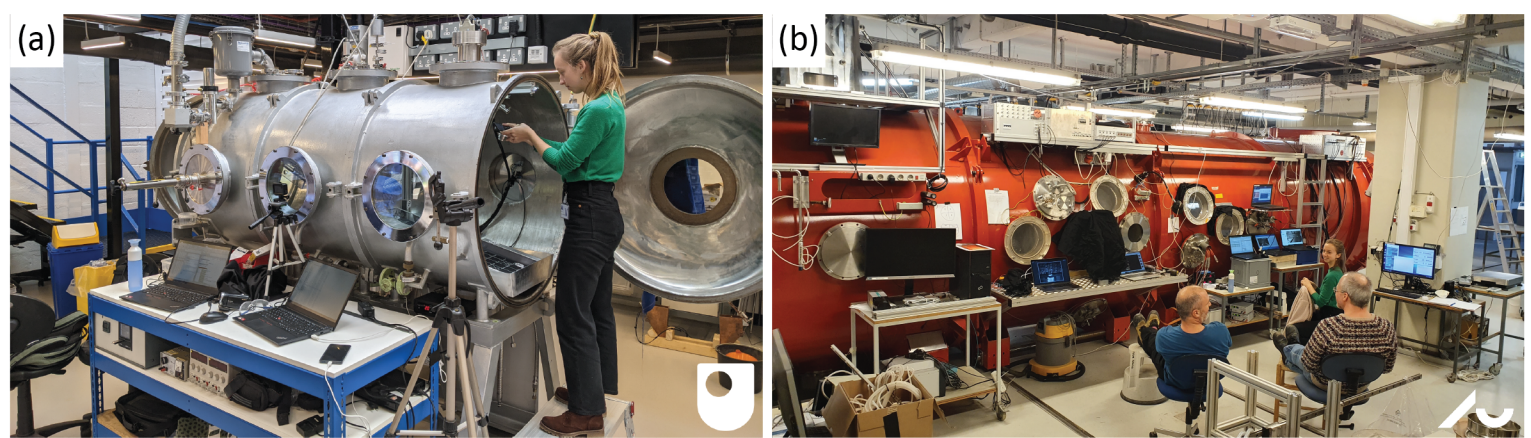


Figure 3.

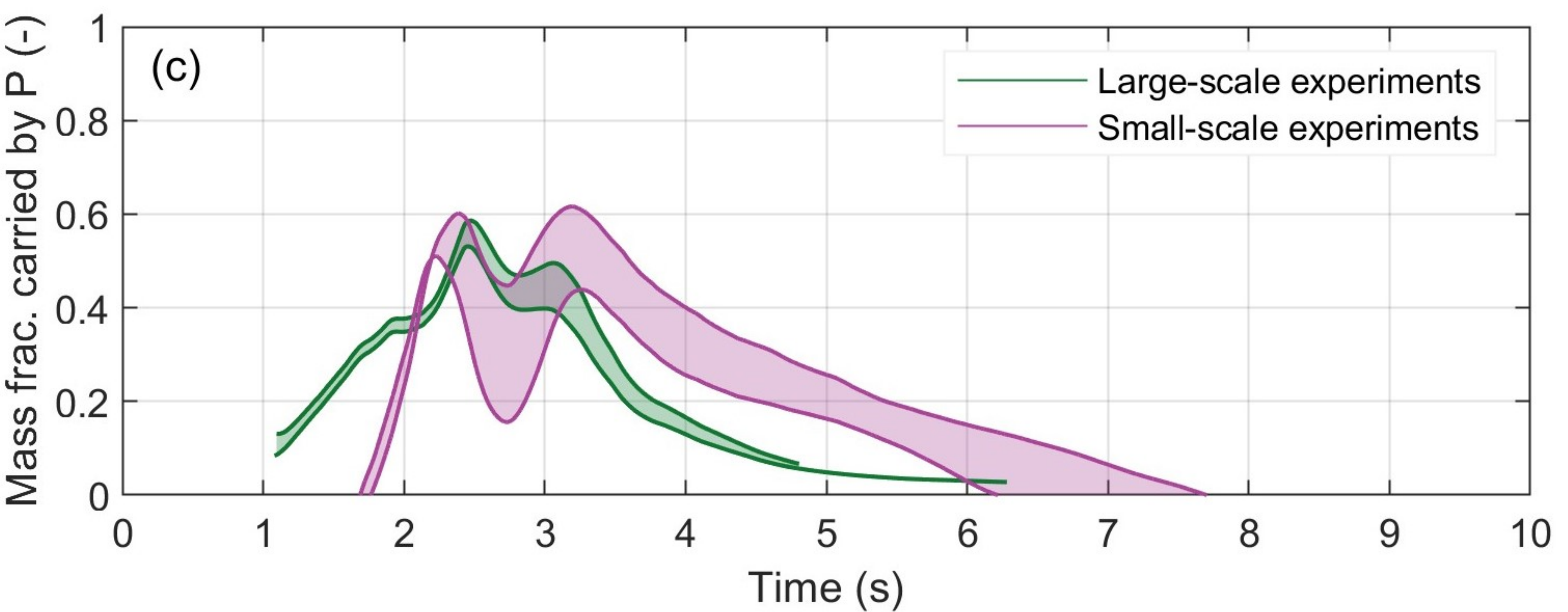
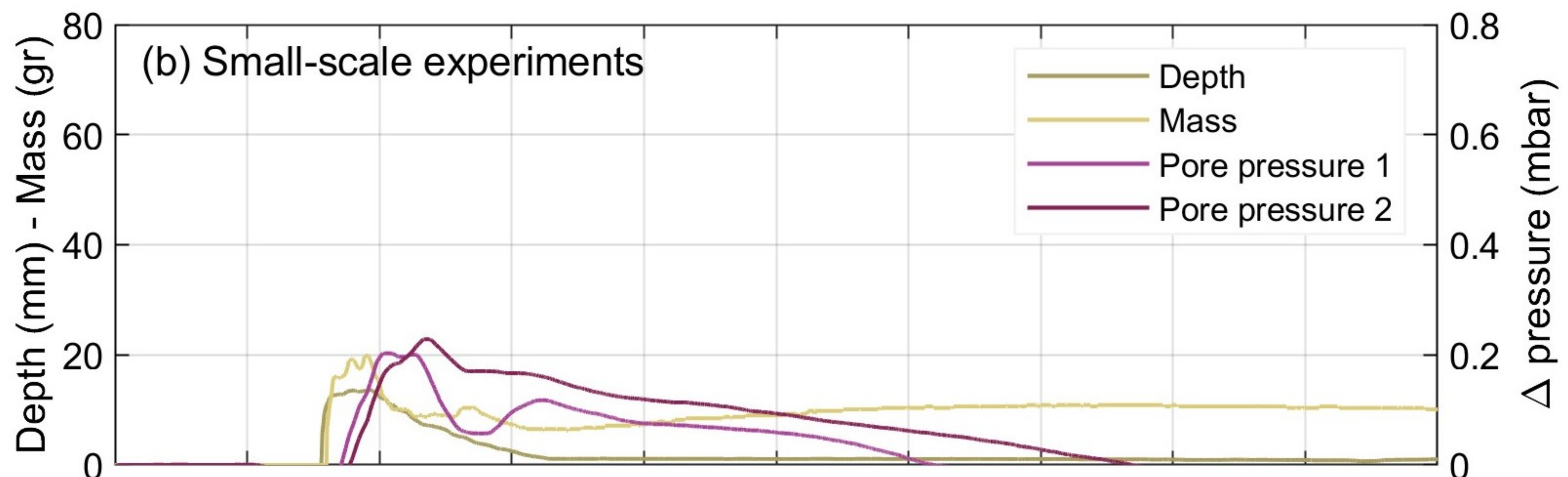
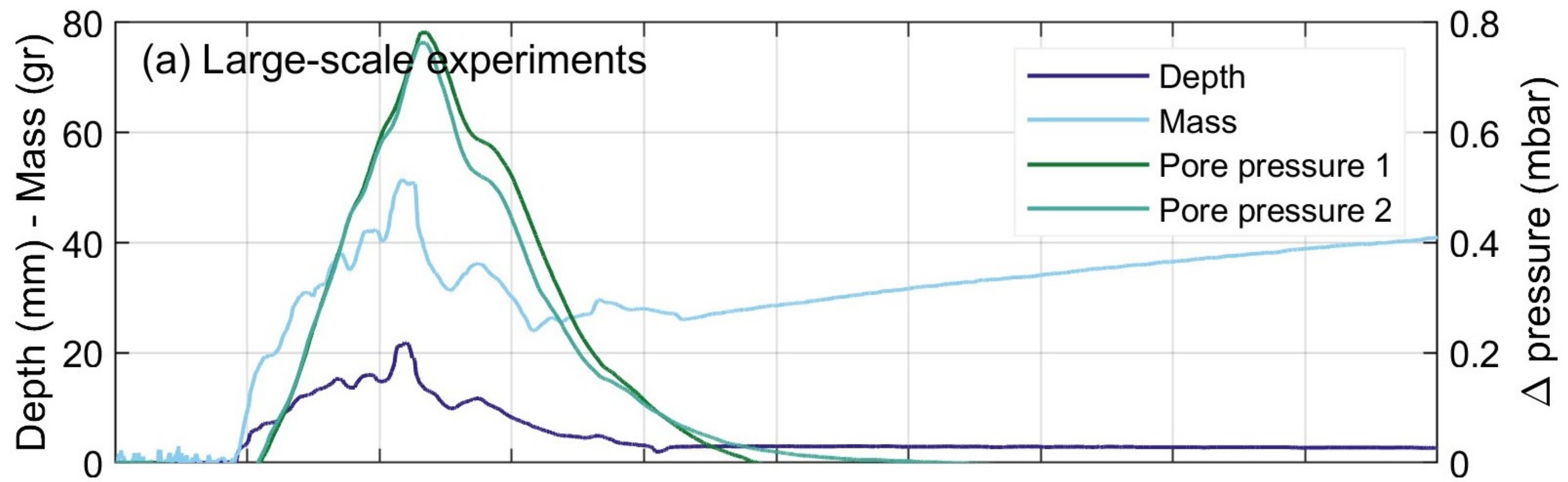


Figure 4.

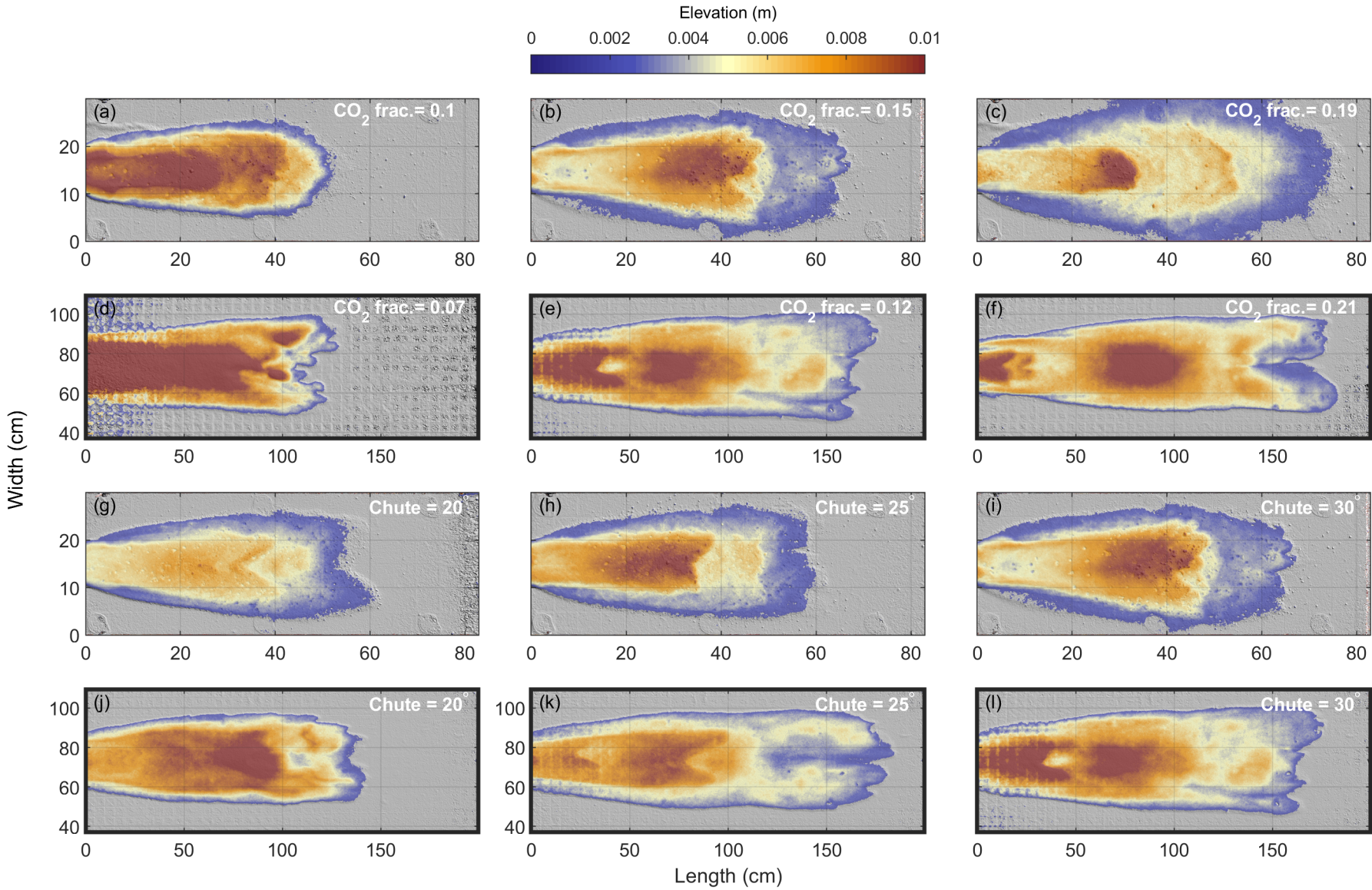


Figure 5.

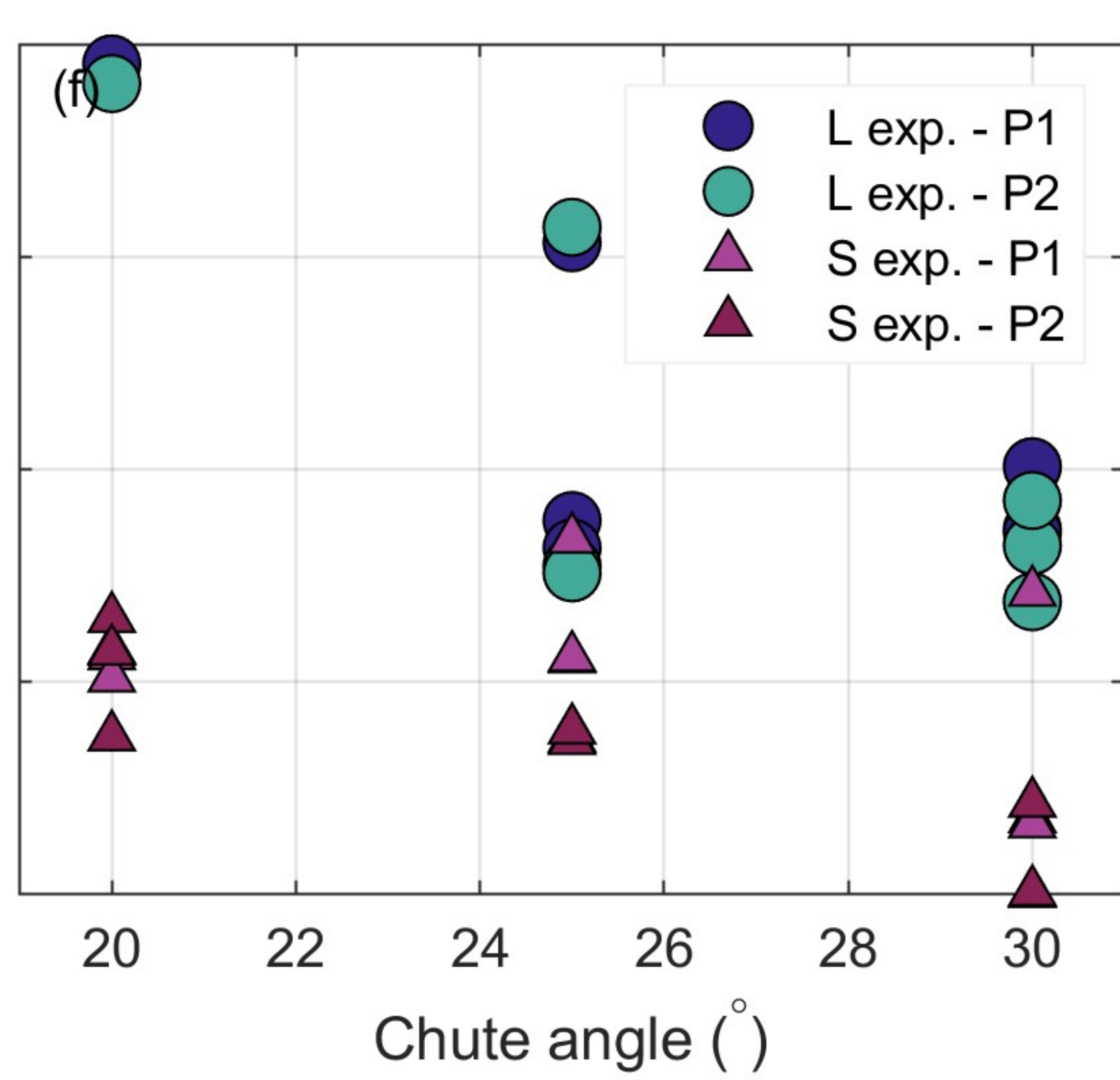
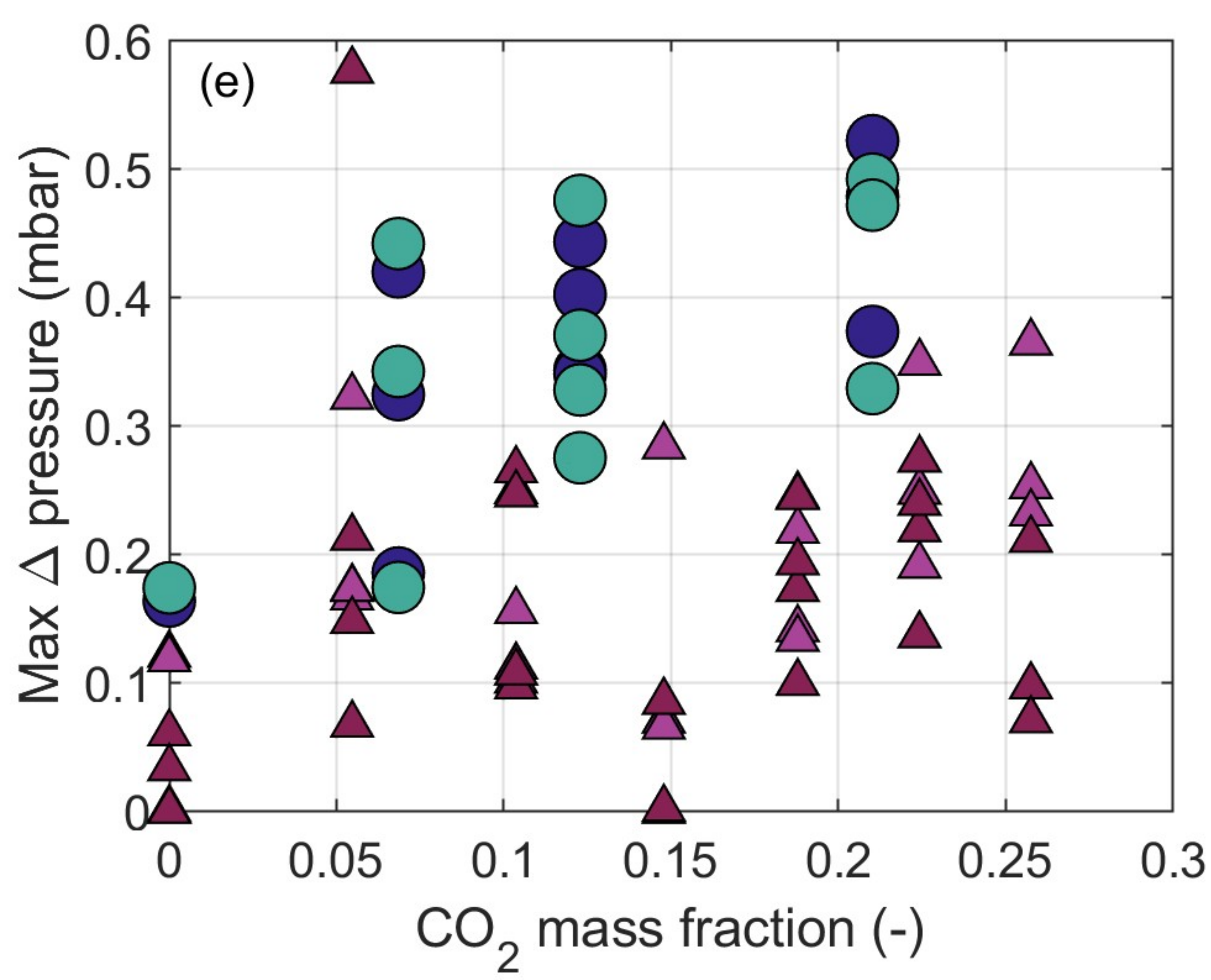
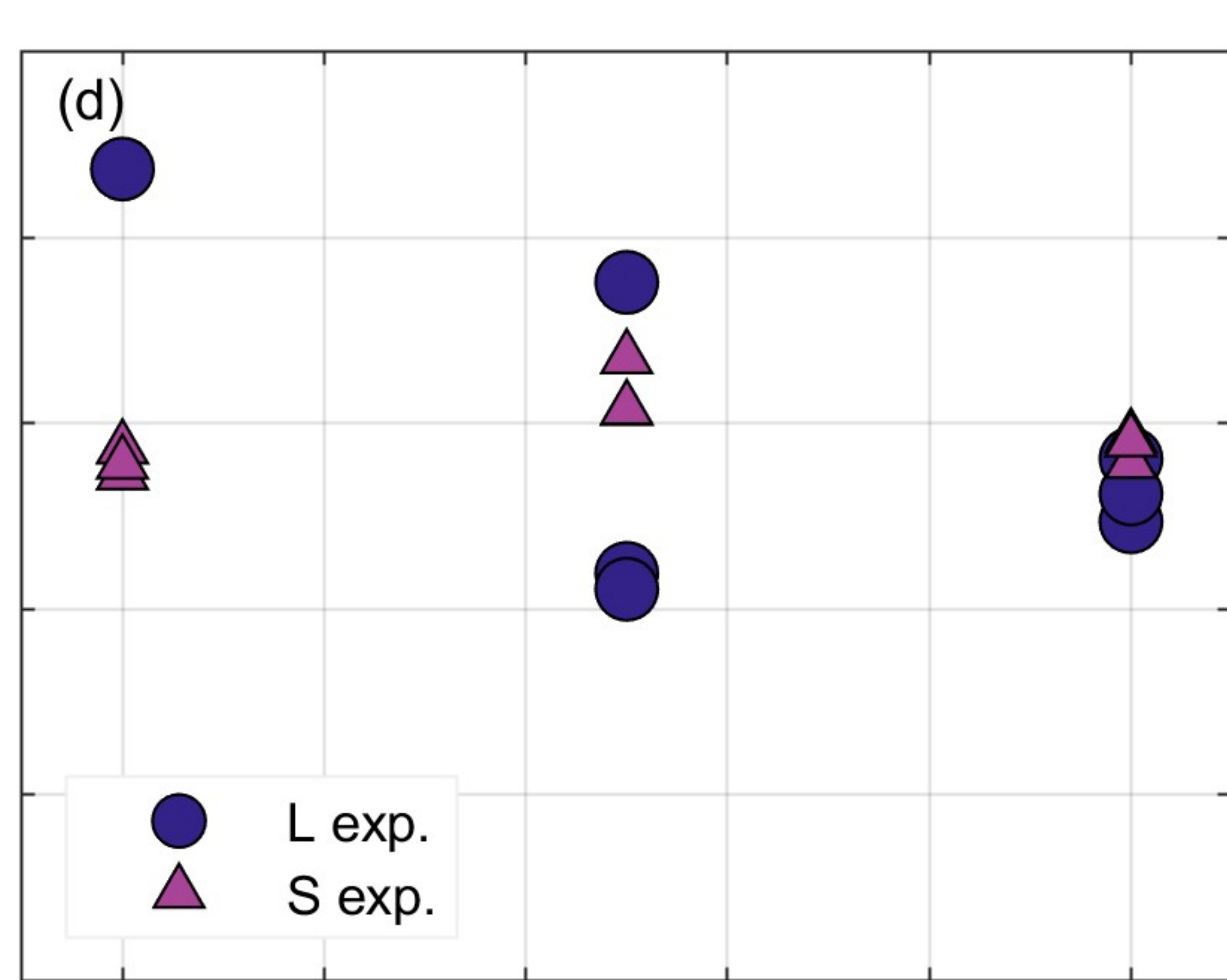
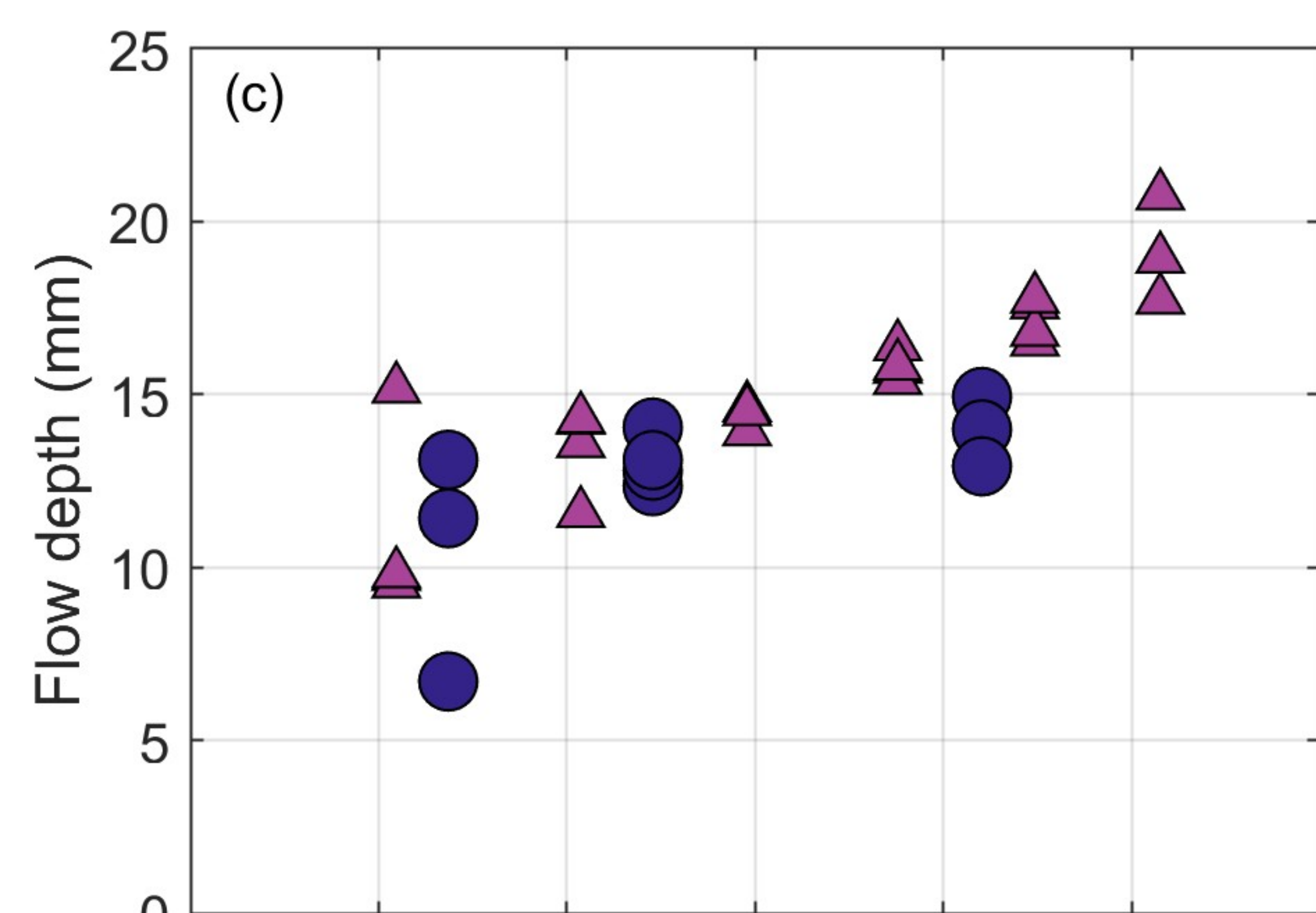
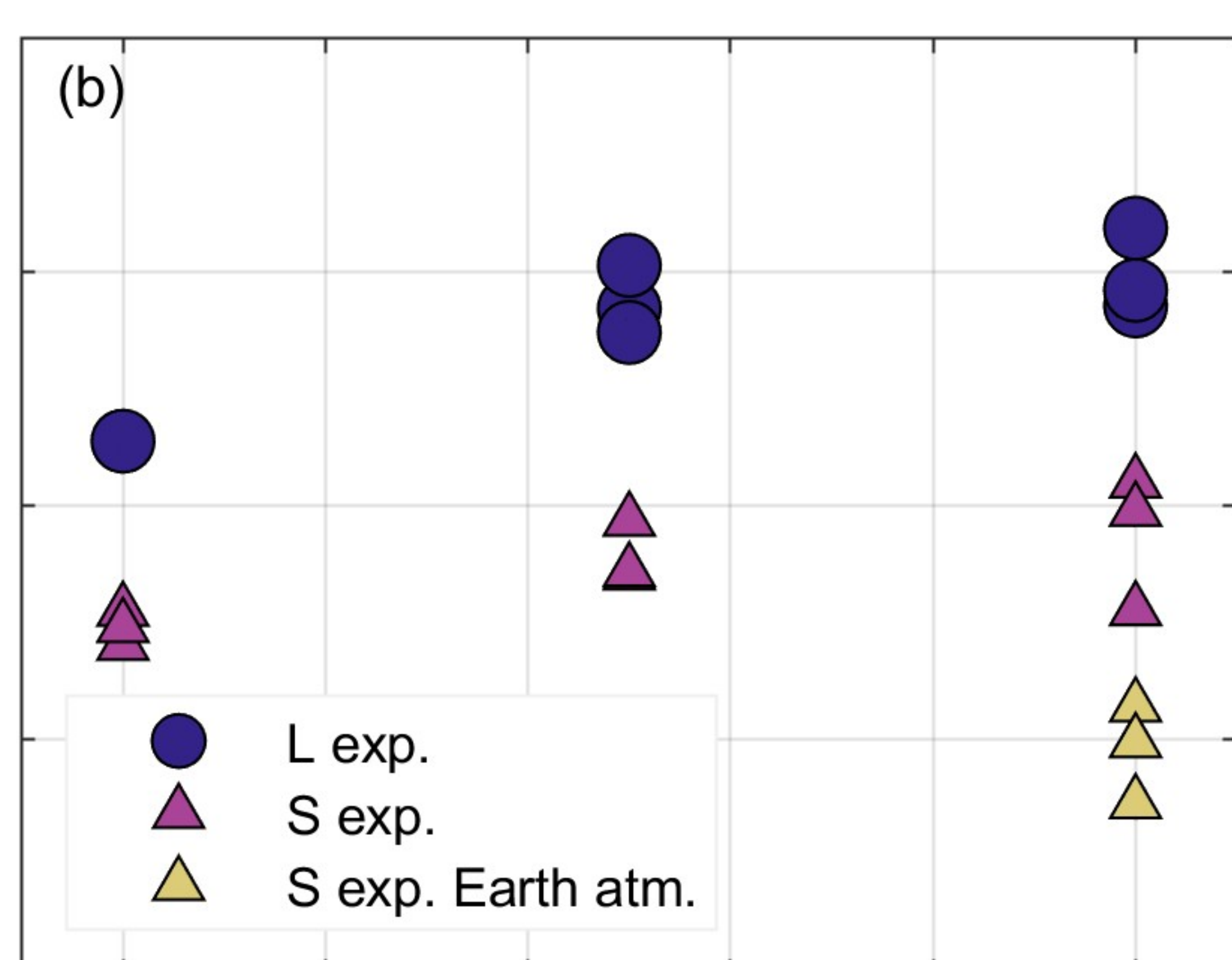
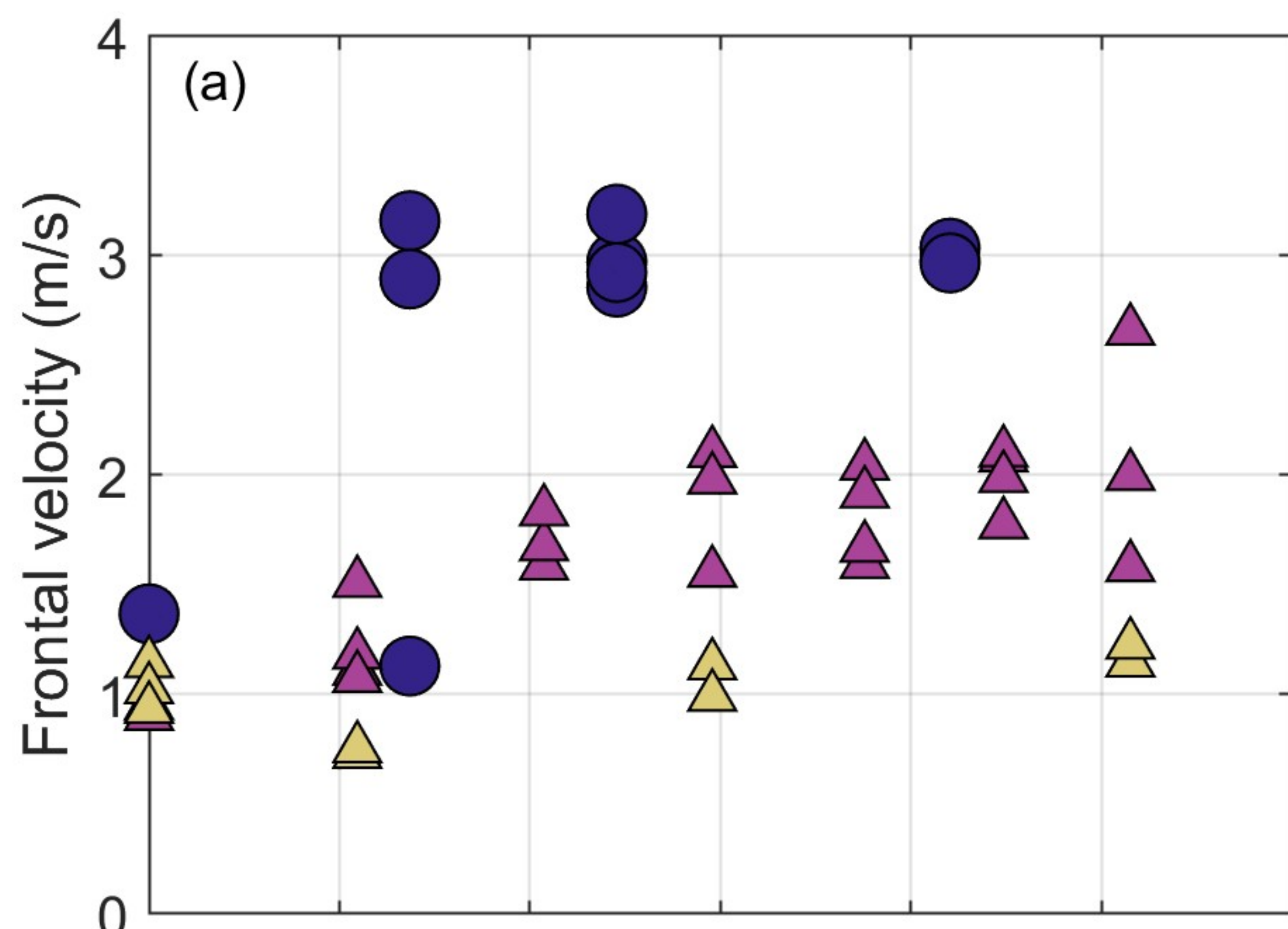


Figure 6.

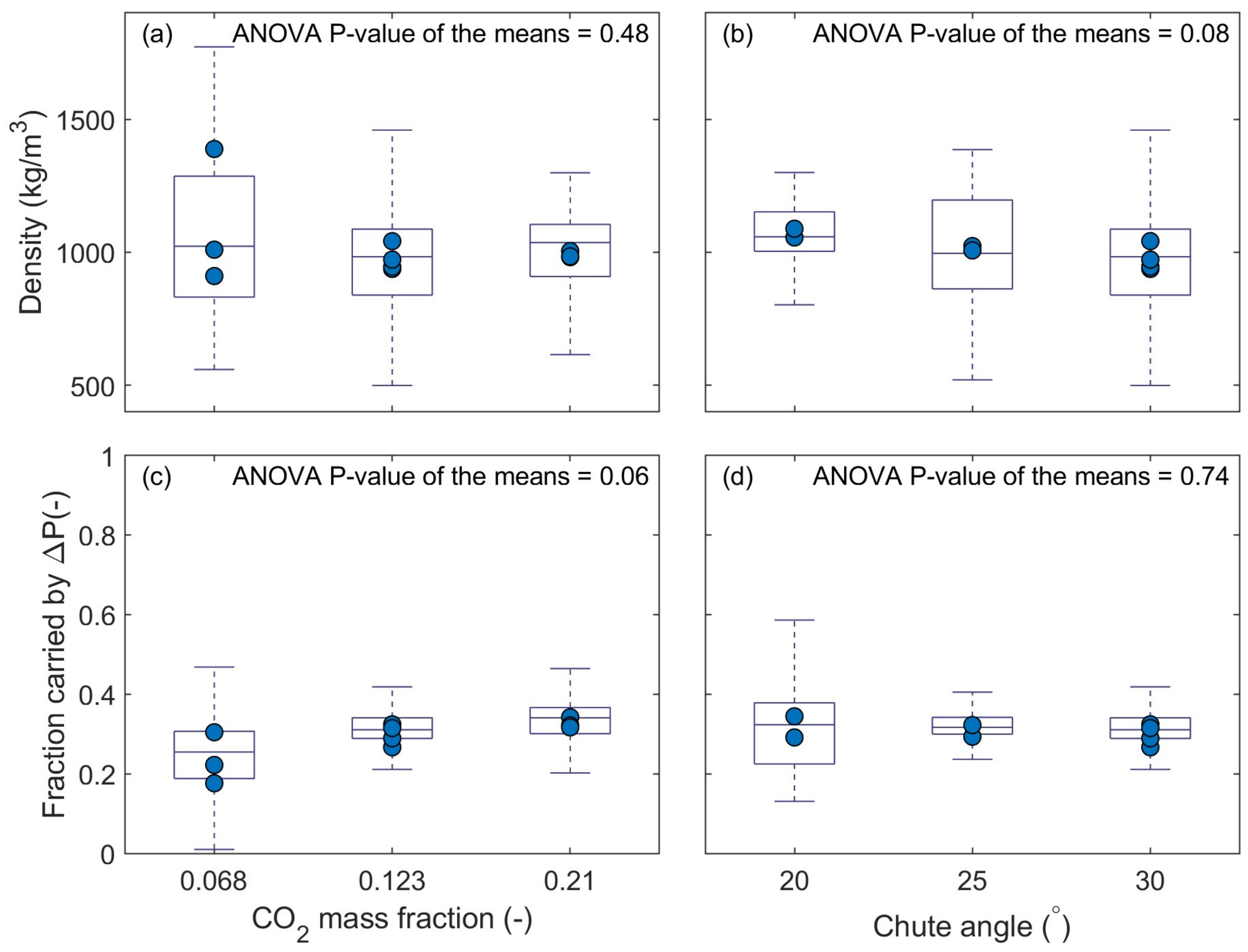


Figure 7.

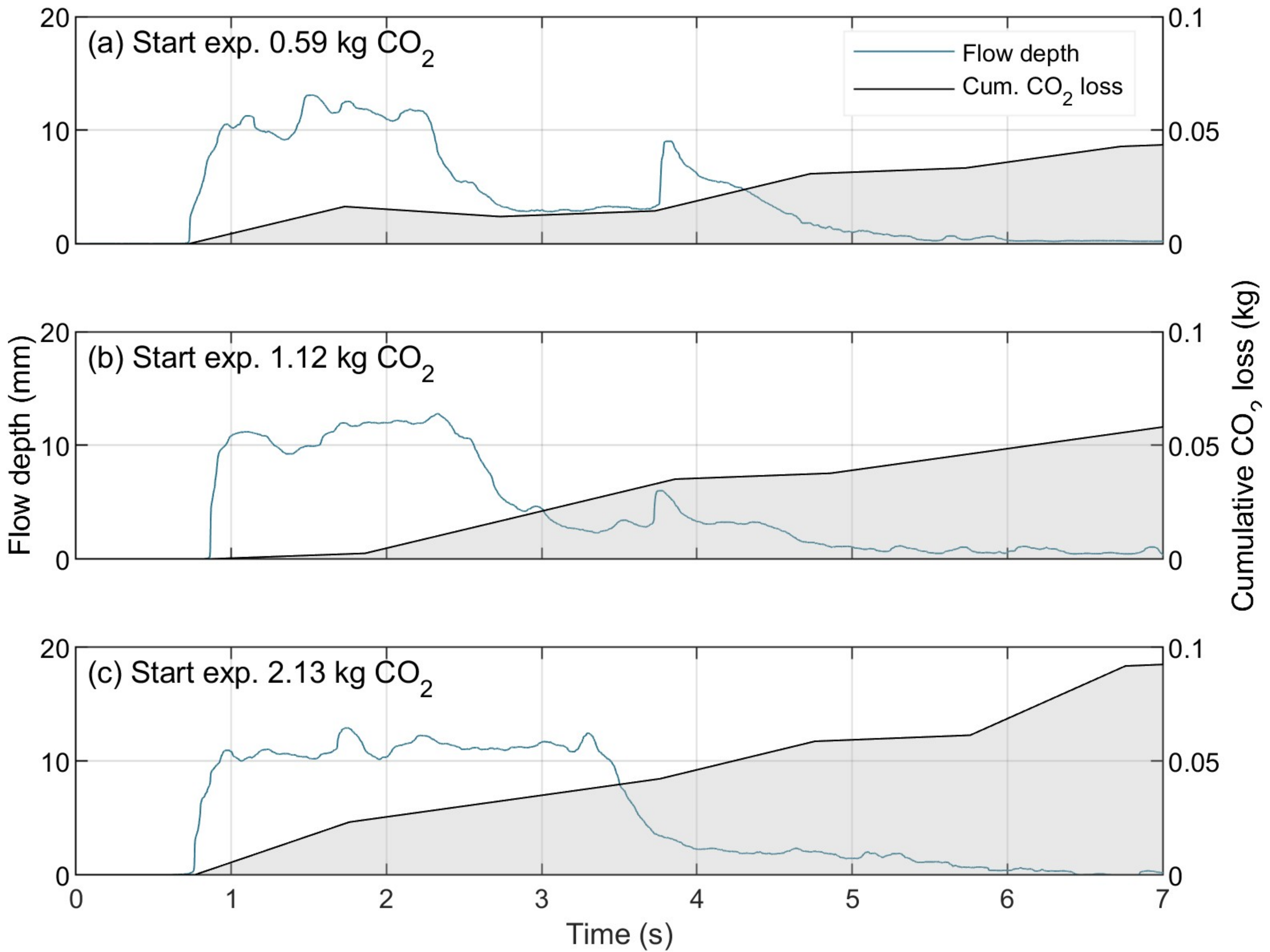


Figure 8.

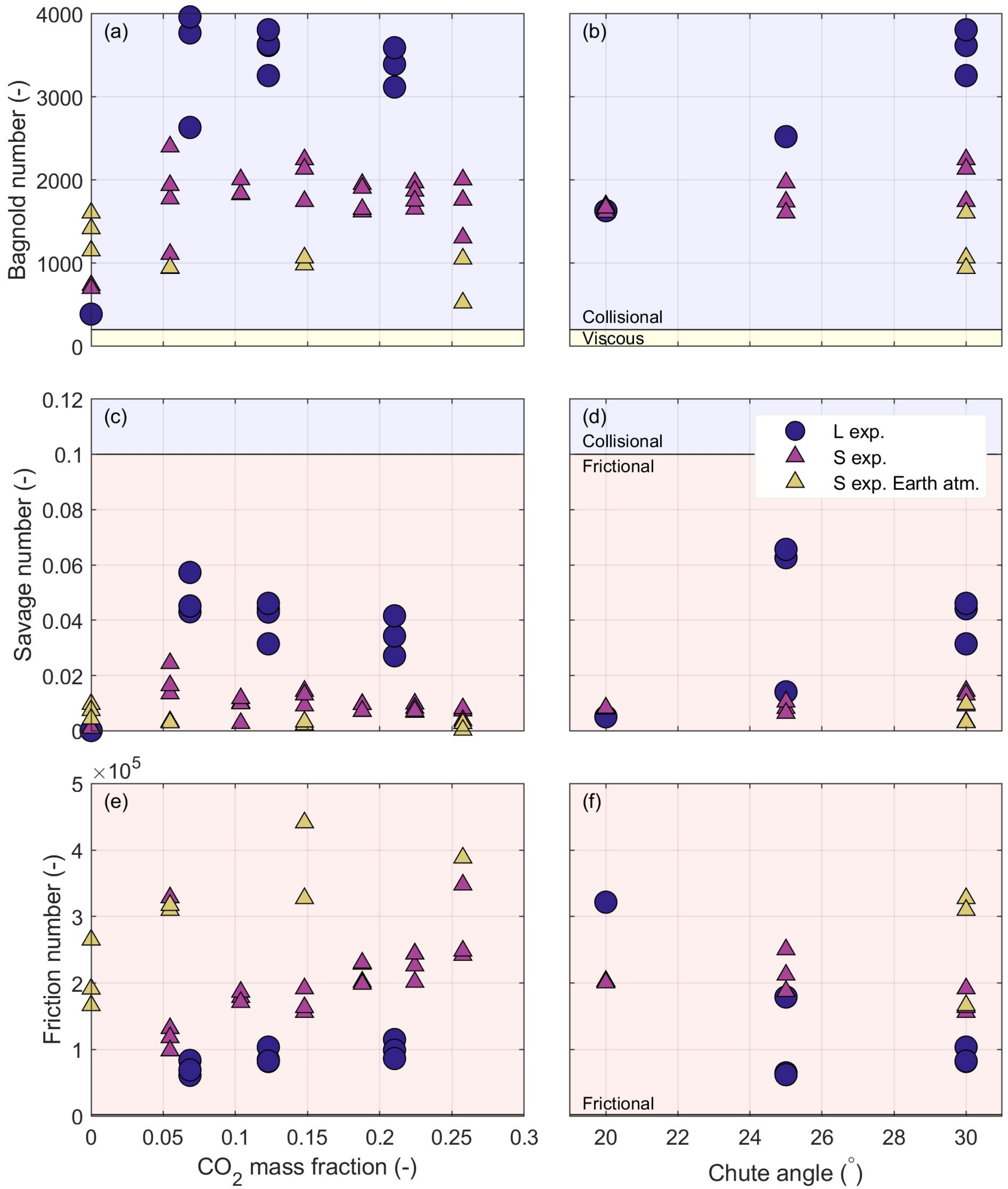


Figure 9.

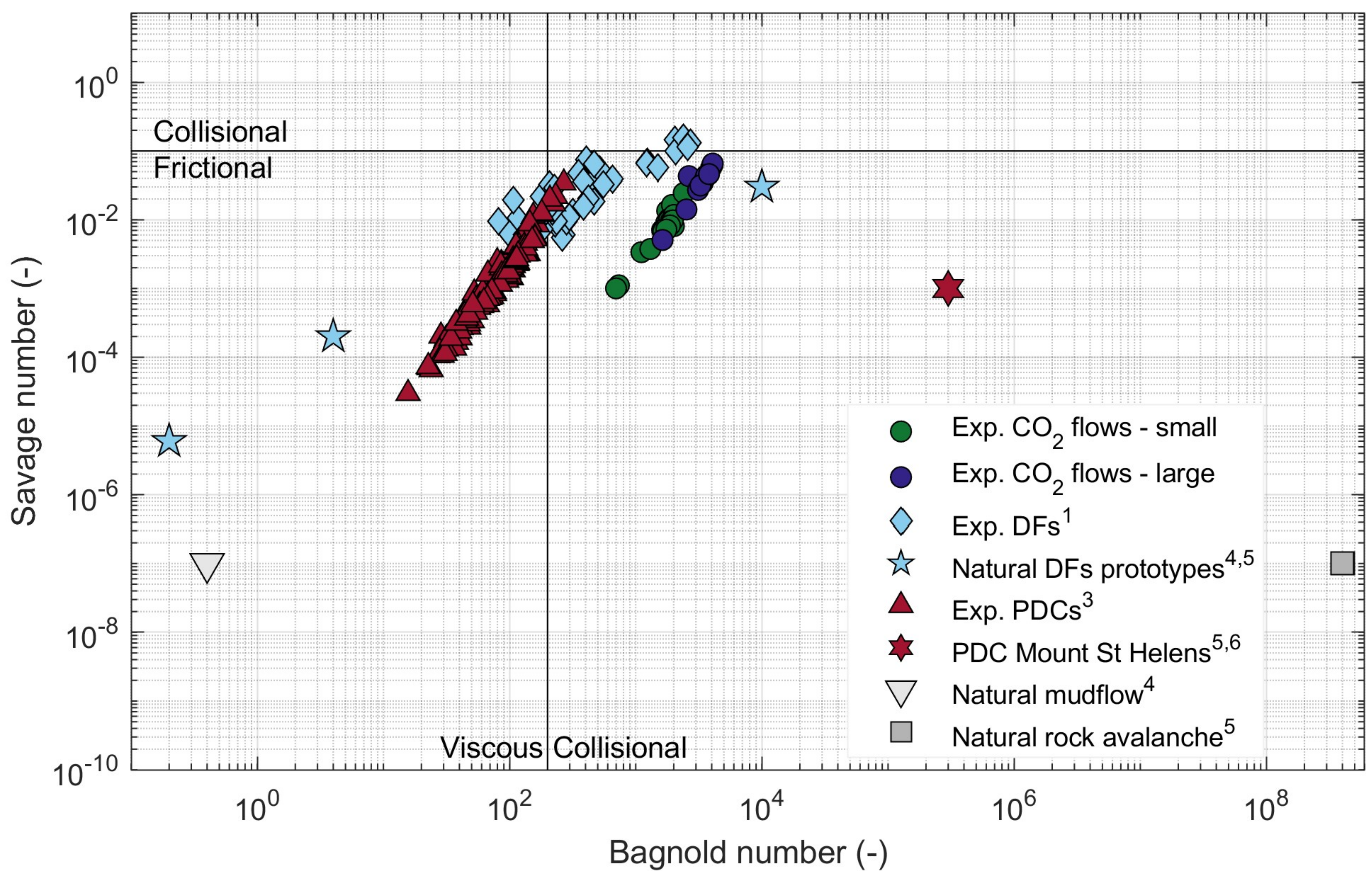


Figure 10.

